Published in final edited form as:
J Am Chem Soc. 2010 September 22; 132(37): 12927–12940. doi:10.1021/ja104107q.

CO and O_2 Binding to Pseudo-Tetradentate Ligand-Copper(I)-Complexes with a Variable N-Donor Moiety: Kinetic/Thermodynamic Investigation Reveals Ligand Induced Changes in Reaction Mechanism

Heather R. Lucas, **Gerald J. Meyer***, and **Kenneth D. Karlin***
Department of Chemistry, The Johns Hopkins University, Baltimore, Maryland 21218

Abstract

The kinetics, thermodynamics, and coordination dynamics for O_2 and CO 1:1 binding to a series of pseudo-tetradentate ligand-copper(I)-complexes ($^{D}LCu^{I}$) to give Cu^{I}/O_2 and Cu^{I}/CO product species are reported. The $^{D}LCu^{I}$ series possess an identical tridentate core structure where the cuprous ion binds to the bispicolylamine (L) fragment. ^{D}L also contains a fourth variable N-donor moiety {D = benzyl (Bz); pyridyl (Py); imidazolyl (Im); dimethylamino (NMe_2-); *tert*-butylphenyl pyridyl (TBP); quinolyl (Q)}. The structural characteristics of $^{D}LCu^{I}$-CO and $^{D}LCu^{I}$ are detailed, with X-ray crystal structures reported for $^{TBP}LCu^{I}$-CO, $^{Bz}LCu^{I}$-CO, and $^{Q}LCu^{I}$. Infrared studies (solution and solid-state) confirm that $^{D}LCu^{I}$-CO possess the same four-coordinate core structure in solution with the variable D moiety 'dangling', i.e. not coordinated to the copper(I) ion. Other trends observed for the present series appear to derive from the degree to which the D-group interacts with the cuprous ion center. Electrochemical studies reveal close similarities of behavior for $^{Im}LCu^{I}$ and $^{NMe2}LCu^{I}$ (as well as for $^{TBP}LCu^{I}$ and $^{Q}LCu^{I}$), which relate to the O_2-binding kinetics and thermodynamics. Equilibrium CO binding data (K_{CO}, ΔH°, ΔS°) were obtained by conducting UV-visible spectrophotometric CO titrations, while CO binding kinetics and thermodynamics (k_{CO} ; $\Delta H^{\ddagger}$, $\Delta S^{\ddagger}$) were measured through variable temperature (193 K – 293 K) transient absorbance laser flash photolysis experiments, λ_{ex} = 355 nm. Carbon monoxide dissociation rate constants (k_{-CO}) and corresponding activation parameters ($\Delta H^{\ddagger}$, $\Delta S^{\ddagger}$) have also been obtained. CO binding to $^{D}LCu^{I}$ follows an associative mechanism with the increased donation from D leading to higher k_{CO} values. Unlike that seen in previous work, the K_{CO} values increased as the k_{CO} and k_{-CO} values declines; the latter decreased at a faster rate. By using the 'flash-and-trap' method (λ_{ex} = 355 nm ; 188 K – 218 K), the kinetics and thermodynamics (k_{O2} ; $\Delta H^{\ddagger}$, $\Delta S^{\ddagger}$) for O_2 binding to $^{NMe2}LCu^{I}$ and $^{Im}LCu^{I}$ were measured and compared to $^{Py}LCu^{I}$. A surprising change in the O_2 binding mechanism was deduced from the thermodynamic $\Delta S^{\ddagger}$ values observed, associative for $^{Py}LCu^{I}$ but dissociative for $^{NMe2}LCu^{I}$ and $^{Im}LCu^{I}$; these results are interpreted as arising from a difference in the timing of electron transfer from copper(I) to O_2 as this molecule coordinates and a tetrahydrofuran (THF) solvent molecule dissociates. The change in mechanism was not simply related to alterations in $^{D}LCu^{II/I}$ geometries or the order that O_2/THF coordinate. The equilibrium O_2 binding constant (K_{O2} ; ΔH°, ΔS°) and O_2 dissociation rate constants (k_{-O2} ; $\Delta H^{\ddagger}$, $\Delta S^{\ddagger}$) were also determined. Overall the results demonstrate that subtle changes in the coordination environment, as occurs over time through evolution in nature or through controlled ligand design in synthetic systems, dictate to a critically detailed level the observed chemistry in terms of reaction kinetics, structure and reactivity, and thus function.

Correspondence: Kenneth D. Karlin, karlin@jhu.edu; Gerald J. Meyer, meyer@jhu.edu.

Supporting Information Available. X-ray data files (CIF), UV-visible data including spectrophotometric CO titrations, Van't Hoff plots, ΔA spectra (O_2 and CO binding), linear [CO] and [O_2] dependence, and Eyring plots are all available free of charge via the Internet at http://pubs.acs.org.

Results reported here are also compared to relevant copper and/or iron biological systems and analogous synthetic ligand-copper systems.

Introduction

A detailed understanding of copper(II/I) protein active site properties and their 1:1 small molecule (CO, O_2, NO) binding characteristics is of importance and has inspired a diverse array of research efforts for biochemists and synthetic bioinorganic chemists alike.[1-6] Research advances through synthetic modeling have helped to gain important insights into copper coordination and reactivity through generation of ligands with precisely optimized formulations and through study of their ligand-copper/small-molecule chemistry. In this context, however, the ability to directly monitor the formation, structures, and subsequent reactivity of Cu^I/O_2 derived primary species, i.e. mononuclear copper(II)-superoxo complexes formulated as (ligand)Cu^{II}-$O_2^{\bullet-}$, is relatively rare.[7-15] Indeed, such species are implicated as key active-site entities in the (bio)chemistry of dioxygen activating copper enzymes.[16-19]

Time resolved laser flash spectroscopy has been widely used to investigate small molecule interactions (CO, O_2, NO, etc.) with natural and synthetic hemes.[20-36] By taking advantage of the extremely short time scale resolution of such photolytic methods, detailed mechanistic information has been achieved. For example, a wealth of knowledge has been gained about both hemoglobin and myoglobin by monitoring photoinitiated CO dissociation from heme-CO in the presence of O_2.[37] Also, in the heme-copper protein cytochrome *c* oxidase (C*c*O; Figure 1), the characterization of photodriven CO transfer (as a surrogate for O_2 and potentially NO[38]) from $heme_{a3}$-CO to Cu_B suggested that the Cu_B site was a "doorway" for small molecules into and out of the heterobimetallic active site.[3,27] Assuming a common O_2 mechanistic pathway and with some indirect evidence existing,[39-41] a Cu^{II}_B-$O_2^{\bullet-}$ intermediate is assumed to precede any $heme_{a3}/O_2$ interactions; a putative peroxo-bridged C*c*O intermediate that was crystallized is shown in Figure 1.

A key aspect for accomplishing such photoinitiated processes is the high binding affinity of heme systems for CO ($K_{CO} > K_{O2}$), as exploited by the "flash-and-trap" experiment pioneered by Gibson and coworkers.[32,33] Similar studies involving CO and O_2 have not been accomplished for the well-characterized type-3 binuclear copper proteins hemocyanin (Hc; Figure 1), tyrosinase (Tyr; widespread monooxygenase, converting phenols to *o*-catechols and *o*-quinones), and catechol oxidase (*o*-catechol → *o*-quinone), mainly due to the opposite behavior, a high stability ($K_{O2} > K_{CO}$) of their 2:1 copper-dioxygen adduct, a dicopper(II)-μ-η^2:η^2-(*side-on*)-peroxo protein species.[3,16,42,43]

Early work established that only one small molecule, CO or O_2, binds per dicopper active site, presumably to Cu_B, and that the close proximity of the two copper centers (Cu_A and Cu_B) enables fast electron-transfer (*et*) for the two-electron reduction of O_2.[3,16,42,43] However, even following photoexcitation and subsequent dissociation of O_2 from oxy-Tyr[44] and/or oxy-Hc,[45,46] a Cu^{II}_B-$O_2^{\bullet-}$ adduct has not been detected and instead only implicated through theoretical modeling.[16,47] Never-the-less, Hirota, Bubacco, and coworkers recently used flash photolysis and complementary K-edge X-ray absorption spectroscopy (XAS) measurements to show that the O_2 binding rate constant (k_{O2}) for a deoxy-Hc was dependent on the copper(I) coordination geometry.[45] In addition, the thermodynamic data ($\Delta H^{\ddagger}$, $\Delta S^{\ddagger}$) they obtained were comparable to those reported for mononuclear synthetic model compounds, which emphasizes the important relationship between synthetic bioinorganic chemistry and metallobiochemistry.

In peptidylglycine α-hydroxylating monooxygenase (PHM), the active-site contains two uncoupled copper centers (Cu…Cu ~ 11 Å; $Cu_A \equiv Cu_H$; $Cu_B \equiv Cu_M$). A copper(II)-superoxo species, which is suggested by some to be the key intermediate that initiates substrate oxidation reactions, has been characterized by X-ray crystallography.[18] This "end-on" η^1 -bound (to Cu_M) "precatalytic" copper-dioxygen adduct is shown in Figure 1. Interestingly, CO binds the catalytic (Cu_M) site as well as to the electron-transfer (Cu_H) center, the latter only if substrate is present.[48,49] Key Cu^I/O_2 1:1 species are also implicated in the enzymatic reactions carried out by copper amine oxidase (CAO)[50-52] and galactose oxidase.[19]

As mentioned, CO heme protein active site interactions have been widely investigated. In addition, the use of CO for investigation of copper proteins provides tremendous insights and fundamental information.[3] The occurrence of detectable and significant variations in active site copper ligation within a given protein has been noted and is also present in proteins from different species or organisms. The ν_{CO} values of carbonmonoxy-copper proteins are highly variable, even when equally coordinated by three imidazolyl N-donors. For example, ν_{CO} values corresponding to the Cu^I-CO adducts of CAO (2061 – 2085 cm^{-1}),[53] the Cu_H-CO site of PHM (2062 cm^{-1}),[48] and the Cu_B-CO sites of C*c*O (2053 – 2063 cm^{-1}),[54-56] nitrite reductase (NiR; 2050 cm^{-1}),[57] and Hc-CO (2043 – 2063 cm^{-1}),[58] exhibit large differences. Such variations in ν_{CO} for N_3Cu^I -CO adducts indicates subtle changes in the local active site environment (e.g., coordination geometry changes, dielectric of the medium, etc.) that alter the copper ion's electron density and thus back-donation to the ligated carbon monoxide. This likely relates to or explains the diverse O_2 and/or NO reactivity amongst various copper proteins.

With this background, one of our goals is to develop an understanding of the kinetics and thermodynamics of copper(I) mediated small molecule interactions, specifically in this report with CO *and* O_2. Carbon monoxide is a good surrogate for dioxygen, even while possessing redox inactive binding characteristics. In addition, copper(I)-carbonyl adducts are typically more stable than their 1:1 copper-dioxygen counterparts and therefore easier to study. By gaining a deeper understanding of how the detailed nature of ligand environment affects CO binding to copper(I), as has been carried out in natural systems, reliable comparisons can be made to Cu^I/O_2 and potentially NO (bio)chemistries.

We previously reported on the CO photodissociation chemistry of a number of cuprous pyridylalkylamine compounds.[59] Effects upon systematic variations in the ligand framework were examined: (i) via changes in the electron-donating ability of TMPA {$\mathbf{^{Py}L}$; tris(2-pyridylmethyl)amine} through addition of 4-pyridyl substituents (*R*-$\mathbf{^{Py}L}$; *R* = $N(CH_3)_2$-, CH_3O-); (ii) by an increase in the chelate ring-size from 5-membered to 6-membered ligand coordination to copper as in PMEA {bis[(3-pyridyl)methyl]-2-(2-pyridyl)ethylamine} vs PMAP {bis[2-(2-pyridyl)ethyl]-(2-pyridyl)methyl-amine}; and (iii) with a change in the donor group moieties as in BQPA {bis(2-quinolylmethyl)(2-pyridylmethyl)amine}. The effort advanced our understanding of the coordination environment required for ligand-copper(I)-carbonyl photodissociation and rebinding of carbon monoxide; tridentate coordination from the tetradentate ligand moieties to the copper(I)-carbonyl center (overall four-coordinate) was required (Chart 1), in which one N-donor moiety was 'dangling', i.e. uncoordinated. Observed variations in kinetics and thermodynamics were shown to derive from particular changes in the copper complex electron-releasing properties, coordination geometry, and/or steric effects.

The subject and direction of the work discussed herein examines the effect of changes in the dangling N-donor moiety within various ligand-copper(I)-complexes ($\mathbf{^{D}LCu^{I}}$) on *both* 1:1 CO and O_2-binding kinetics and thermodynamics as well as CO and O_2 coordination

dynamics. Variable temperature transient absorbance (TA) laser flash photolysis in tetrahydrofuran (THF) solvent has been employed. The $^{\mathbf{D}}\mathbf{L}$ ligand series consists of potentially tetradentate ligands with the same PY1 {**L** ; bis(2-pyridylmethyl)amine} core, however with variable N-donor moieties (**D**), see Chart 1. For the studies of CO binding, a tridentate ligand species $^{\mathbf{Bz}}\mathbf{L}$ was also examined as a "standard" for comparison.[25] As will be described, drastic differences in Cu^{I}-CO and Cu^{I}-O_2 chemistry result from seemingly minor changes in the $^{\mathbf{D}}\mathbf{LCu^{I}}$ ligand framework.

Experimental

See Supporting Information for details concerning Materials and Methods, references to syntheses of previously published ligands and complexes along with synthetic procedures for new compounds.

Results

Synthesis of Ligand-Copper(I) ($^{D}LCu^{I}$) and Ligand-Copper(I)-Carbonyl ($^{D}LCu^{I}$-CO) Complexes

The ligands ($^{\mathbf{D}}\mathbf{L}$) used in the present study were previously reported and characterized in detail (Chart 1).[60-65] The ligand-copper(I) complexes as $B(C_6F_5)_4^-$ salts ($^{\mathbf{D}}\mathbf{LCu^{I}}$) were straightforwardly prepared by addition of $[Cu^{I}(MeCN)_4]B(C_6F_5)_4$ to the appropriate ligand in deoxygenated Et_2O and isolated by slow precipitation in dry air-free pentane under an argon atmosphere.[8,60,64-66] The $B(C_6F_5)_4^-$ counteranion was chosen to afford greater solubility in tetrahydrofuran (THF) solvent.

The presence of coordinated acetonitrile (CH_3CN) in the isolated copper(I) complexes of $^{\mathbf{Py}}\mathbf{LCu^{I}}$, $^{\mathbf{Im}}\mathbf{LCu^{I}}$, $^{\mathbf{NMe_2}}\mathbf{LCu^{I}}$, and $^{\mathbf{Bz}}\mathbf{LCu^{I}}$ was confirmed through elemental (C, H, N) combustion analysis and ^{1}H-NMR spectroscopy studies in deuterated nitromethane (CD_3NO_2).[8,60,64,65] The X-ray crystal structures of $^{\mathbf{Bz}}\mathbf{LCu^{I}}$ and the ClO_4^- salts of $^{\mathbf{NMe_2}}\mathbf{LCu^{I}}$ and $^{\mathbf{Py}}\mathbf{LCu^{I}}$ were previously reported with each containing an exogenously derived CH_3CN molecule.[60,62,67] As expected for a tridentate ligand system, $^{\mathbf{Bz}}\mathbf{LCu^{I}}$ binds CH_3CN the strongest as supported by the shorter $Cu–N_{nitrile}$ bond distance of 1.900(4) Å versus a value of 2.038(2) Å for $^{\mathbf{NMe_2}}\mathbf{LCu^{I}}$ and 1.990(12) Å for $^{\mathbf{Py}}\mathbf{LCu^{I}}$, the complexes with tetradentate N4 ligation. Acetonitrile does not coordinate to $^{\mathbf{TBP}}\mathbf{LCu^{I}}$ and $^{\mathbf{Q}}\mathbf{LCu^{I}}$ based on the characterization methods described above and X-ray structural characterization, *vide infra*.

Ligand-copper(I)-carbonyl complexes ($^{\mathbf{D}}\mathbf{LCu^{I}}$**-CO**) were formed *in situ* through vigorous CO bubbling into dry THF solutions. $^{\mathbf{TBP}}\mathbf{LCu^{I}}$**-CO** and $^{\mathbf{Bz}}\mathbf{LCu^{I}}$**-CO** were isolated as overall four-coordinate species, i.e., possessing a dangling ligand donor arm (*vide infra*), following dissolution of $^{\mathbf{TBP}}\mathbf{LCu^{I}}$ and $^{\mathbf{Bz}}\mathbf{LCu^{I}}$ in CO saturated Et_2O and layering with pentane for slow diffusion.[68] In a previous study, $^{\mathbf{Py}}\mathbf{LCu^{I}}$**-CO** was isolated as a five-coordinate species, i.e., with all ligand N donors coordinated.[59]

X-ray Crystallography of $^{TBP}LCu^{I}$-CO, $^{Bz}LCu^{I}$-CO, $^{Q}LCu^{I}$

ORTEP diagrams of $^{\mathbf{TBP}}\mathbf{LCu^{I}}$**-CO** (A) and $^{\mathbf{Bz}}\mathbf{LCu^{I}}$**-CO** (B) are shown in Figure 2 and that for $^{\mathbf{Q}}\mathbf{LCu^{I}}$ is given in Figure 3; selected bond lengths and angles for all are provided in the figure caption.[68] Both ligand-copper(I)-carbonyl structures display an overall four-coordinate geometry consisting of the copper(I) ion coordinated by the apical alkylamino nitrogen, two pyridyl donors, and the carbon from a coordinated CO molecule. The $N_{pyridyl}–Cu–N_{amine}$ angles of ~81° are rather severe in comparison to other structurally characterized four-coordinate copper(I) carbonyl complexes which have average N–Cu–N bond angles of ~95°.[59,69-75] The Cu-C bond length is shorter (stronger) for $^{\mathbf{TBP}}\mathbf{LCu^{I}}$**-CO** (1.801 Å) in

comparison to that observed in ^{Bz}**LCu^{I}-CO** (1.815 Å), possibly due to an indirect increase in overall electron density in the former complex, with the difference being a *tert*-butylphenyl (*tbp*) substituted pyridine vs. benzyl substituent on the **L** tridentate moiety, see Chart 1.

A tridentate (N_3) coordination mode for ^{TBP}**LCu^{I}-CO** is of interest due to the tetradentate (N_4) nature of ^{TBP}**L**; the 6-*tbp*-substituted pyridyl arm dissociates, i.e. is dangling, due to the increased steric constraints. However in the absence of CO all three pyridyl donors as well as the bridgehead alkylamine coordinate to the copper(I) ion, as supported by the known X-ray crystal structure of ^{TBP}**LCu^{I}**.[64] The coordination sphere of ^{TBP}**LCu^{I}** did not include a coordinated acetonitrile molecule as is generally observed for analogous ligand-copper(I) complexes, *vide supra*.

Similar structural characteristics have been reported based on X-ray crystallographic analysis of the copper(I) complex and copper(I)-carbonyl adduct of BQPA.[59,63,76] For [Cu^{I}(bqpa)]B(C_6F_5)$_4$, all four N-donor moieties coordinate to the copper(I) ion and one quinolyl donor arm dissociates upon coordination of CO or triphenylphosphine (PPh_3).[63] As shown in Figure 3, the X-ray crystal structure of ^{Q}**LCu^{I}** is four-coordinate with both pyridyl donors, the quinolyl donor, and the bridgehead alkylamine coordinated to the cuprous center. An X-ray crystal structure of ^{Q}**LCu^{I}-CO** has not been obtained but IR spectroscopic data supports a tridentate ligand coordination in which the quinolyl arm is dangling, *vide infra*.

Infrared Spectroscopy (ν_{CO}: Solution and Solid State)

The solution (THF) and solid-state (Nujol mull) ν_{CO} values of the ligand-copper(I)-carbonyl complexes (^{D}**LCu^{I} -CO**) were determined in order to gauge the ligand-N-donor ability of the variable D-moiety as well as to elucidate potential differences in coordination number and/or the overall geometry. As described above, in part, the CO stretching frequencies (ν_{CO}) of synthetic copper(I)-carbonyl complexes and carbonmonoxy- copper proteins are found to be in the range ν_{CO} = 2035 – 2137 cm^{-1}. [3,73,77-82] Notably, the characteristic ν_{CO} values of copper(I)-carbonyl proteins coordinated by three imidazolyl N-donors are usually $\Delta\nu_{CO}$ = 20 – 40 cm^{-1} lower than synthetic species with three N-donors. [3,79] This suggests that copper protein histidine imidazole groups are exceptionally strong donors and relative to most synthetic copper(I)-carbonyl complexes, this leads to weaker C–O (but stronger Cu-C) bonds.

Solution-State IR Spectroscopic and Structural Properties—As discussed in the Introduction (Chart 1), previous work established that an equilibrium mixture of four- ($^4\nu_{CO}$ = 2090 cm^{-1}) and five- ($^5\nu_{CO}$ = 2077 cm^{-1}) coordinate copper(I)-carbonyl isomers exist for ^{Py}**LCu^{I}-CO** in THF solvent, Table 1 and Chart 1. Similarly, an equilibrium mixture of ^{Im}**LCu^{I}-CO** isomers exist in THF, $^4\nu_{CO}$ = 2087 cm^{-1} and $^5\nu_{CO}$ = 2063 cm^{-1}. The lower energy shift of $\Delta^5\nu_{CO}$ = 14 cm^{-1} for ^{Im}**LCu^{I}-CO** isomer in comparison to ^{Py}**LCu^{I}-CO** indicates that the imidazole in ^{Im}**L** is a stronger donor for copper(I) than the pyridine in ^{Py}**L**. However, the hard aliphatic amine group within ^{NMe2}**LCu^{I}-CO** does not ligate at all in THF solution, as indicated by the single CO stretch at 2090 cm^{-1}.

Consistent with their X-ray crystal structures, ^{TBP}**LCu^{I}-CO** and ^{Bz}**LCu^{I}-CO** are four-coordinate structures in THF solution with $^4\nu_{CO}$ values of 2091 cm^{-1} and 2093 cm^{-1} respectively, see Table 1. THF solution data for ^{Q}**LCu^{I}-CO** reveals the same N_3Cu^{I}-CO coordination based on the $^4\nu_{CO}$ value. Overall, the CO stretching frequencies for all four-coordinate ^{D}**LCu^{I}-CO** solution complexes are approximately equal, $^4\nu_{CO}$(avg) = 2091 cm^{-1}, indicating that the dangling arm throughout the series must be the **D**-donor moiety, as depicted in Chart 1.

Solid-State IR Spectroscopic and Structural Properties—The $^4\nu_{CO}$ values of the isolated **^{Im}LCu^I-CO** and **^{NMe2}LCu^I-CO** species were both centered at 2097 cm^{-1} in Nujol mull spectra suggesting that the imidazole or aliphatic dimethylamine donor moieties do not coordinate in the static solid-state structure. Since these values are higher than the solution state $^4\nu_{CO}$ values, the **^{D}L** ligation may be somewhat more two-coordinate in nature, i.e., perhaps the aliphatic amine nitrogen is less strongly bound than for the other cases (Chart 2). In the solid state, **^{Py}LCu^I-CO** has an overall five-coordinate structure.[59]

For **^{Im}LCu^I-CO**, an additional very low energy and intensity CO stretch at 2035 cm^{-1} is observed in the solid-state. Such a low ν_{CO} value suggests a coordination environment with anionic ligand donors, or three strong non-chelating N donors, as is known elsewhere.[3,78] In previous work, the electron-donating ability of the four-coordinate *R*- **^{Py}L** ligand series was increased by introduction of *para*-substituents such as *R* = $N(CH_3)_2$- and CH_3O- (Chart 2)[59]. Here, ν_{CO} values shifted to lower energy by 14 to 28 cm^{-1}, e.g., ν_{CO} = 2049 cm^{-1} for $[Cu^I(NMe_2$- **^{Py}L**$)(CO)]^+$ in THF. To explain the very low 2035 cm^{-1} ν_{CO} value, we suggest that the dangling imidazolyl moiety of **^{Im}LCu^I-CO** may coordinate to a different **^{Im}LCu^I** complex, forming a dimeric structure, see Chart 2 below. Pyridyl π–π stacking may facilitate formation of such a structure, as has been observed elsewhere for copper(I) structures.[83-85]

Electrochemical Studies

Copper(II/I) redox chemistry was examined through cyclic voltammetry measurements carried out on the ligand-copper(I)-complexes (**^{D}LCu^I**). Quasi-reversible single electron-transfer processes ($i_{pc}/i_{pa} \approx 1$) with peak-to-peak separations between ΔE = 75 – 155 mV were observed (Table 1). The Cu^{II}/Cu^I redox potentials, i.e. electron transfer, are largely affected by structural alterations prompted by changes in oxidation states as well as steric hindrance induced by ligand variations. Overall, the trend of $Cu^{II/I}$ half-wave potentials ($E_{1/2}$) were similar to the trend of the $^4\nu_{CO}$ values of **^{D}LCu^I-CO** species in THF, see Table 1. Ligand-copper-complexes with more negative $E_{1/2}$ values favor a higher oxidation state (Cu^{II}) and suggest a more donating ligand system. For example, the formally tridentate **^{Bz}LCu^I**, has the highest redox potential of −225 mV, hence favoring a lower oxidation state.

The same $E_{1/2}$ values were measured for **^{Q}LCu^I** and **^{TBP}LCu^I** at −325 mV and their peak-to-peak separation was also about the same, ΔE_{avg} = 115 mV. These results suggest that the steric influence of the quinoline donor and 6-*tbp*-subsituent are very similar. The same $E_{1/2}$ values were also measured for **^{Im}LCu^I** and **^{NMe2}LCu^I** at −445 mV, which was surprising because of their different static copper(II) structures. The X-ray crystal structure of $[Cu^{II}(^{NMe2}L)(Cl)]^{2+}$ reveals a distorted square pyramidal coordination geometry, τ = 0.26.[62,86] The τ structural parameter is 0.00 for a perfect square pyramidal structure and l.00 for a perfect trigonal bipyramidal coordination geometry.[86,87] By contrast, $[Cu^{II}(^{IM}L)(CH_3CN)]^{2+}$ displays a trigonal bipyramidal static structure, τ = 0.86.[65,86]

Since $[Cu^{II}(^{Py}L)(CH_3CN)]^{2+}$ has an almost perfect trigonal bipyramidal static structure, τ = 0.96,[67,86] the same degree of structural rearrangement would be expected to occur upon oxidation of **^{Im}LCu^I**and **^{Py}LCu^I**. Both of their cuprous-acetonitrile structures are assumed to be very similar based on their related **^{D}LCu^I-CO** $^4\nu_{CO}$ values. However, the $E_{1/2}$ values are quite different for **^{Im}LCu^I** (107 mV) and **^{Py}LCu^I** (76 mV) suggesting that the *in situ* copper(II) structures are different. The $E_{1/2}$ value of **^{Im}LCu^I** (and **^{NMe2}LCu^I**) in comparison to **^{Py}LCu^I** (−410 mV) is 35 mV more negative, therefore the latter is easier to reduce.

CO Equilibrium Binding and Thermodynamic Parameters (K_{CO}: ΔH°, ΔS°)

The equilibrium CO binding constants (K_{CO}, Scheme 1) and corresponding thermodynamic parameters (ΔH°; ΔS°) were determined by variable temperature monitoring of THF solvent reactions of CO with ^{D}**LCu^{I}** to form ^{D}**LCu^{I}-CO.**[59] Throughout the entire series (Table 2), K_{CO} increases are accompanied by decreasing (more favorable) enthalpies but less favorable (decreasing) reaction entropies. This behavior is typical, as enhanced binding can be described as being "tighter". UV-visible spectral data representative of the conversion of ^{TBP}**LCu^{I}** to ^{TBP}**LCu^{I}-CO** are shown in Figure 4; data corresponding to all other species are found in the Supporting Information.

CO Photodissociation and Rebinding Kinetics

The kinetics and thermodynamics of CO binding to ^{D}**LCu^{I}** were measured through variable temperature (20 to −80°C) transient absorption (TA) laser flash photolysis experiments.[15,59] Absorption difference spectra, Abs{[^{D}**LCu^{I}**] – [^{D}**LCu^{I}-CO**]}, calculated from steady-state absorption experiments were in agreement with observed transient data collected within the range λ_{mon} = 325 – 700 nm; see Figure 5 for ΔA spectra corresponding to photodissociation of CO from ^{TBP}**LCu^{I}-CO**. The subsequent rebinding of CO followed a first-order kinetic model. Bimolecular rate constants (k_{CO}) for ^{D}**LCu^{I}-CO** formation were calculated based on [CO] dependence studies.[59] Complementary activation ($\Delta H^{\ddagger}$; $\Delta S^{\ddagger}$) parameters were calculated by determination of k_{CO} at variable temperatures and through Eyring analysis.[59]

In all cases, CO (re)binding to ^{D}**LCu^{I}** follows an associative mechanism as suggested by the k_{CO} associated negative reaction entropies ($\Delta S^{\ddagger}$) in the range −40 to −76 J mol^{-1} K^{-1}, see Table 2. Furthermore, the nearly identical thermodynamic (ΔS°) and activation ($\Delta S^{\ddagger}$) entropies along the ^{D}**L** series of complexes suggest a late transition state; the rate determining step involves an intermediate that is structurally similar to the final carbonylated product. Following CO photodissociation, the dangling N-donor arm of ^{D}**LCu^{I}-CO** binds to the open coordination site of the cuprous ion and must dissociate before CO can rebind.

Thermal ^{D}LCu^{I}-CO Dissociation Kinetics

With K_{CO} and k_{CO} values determined experimentally, the thermal CO dissociation rate constants (k_{-CO}) and corresponding activation parameters ($\Delta H^{\ddagger}$, $\Delta S^{\ddagger}$) were calculated.[59] As expected, the k_{-CO} value increases with decreasing reaction enthalpies ($\Delta H^{\ddagger}$) and increasing entropic ($\Delta S^{\ddagger}$) values. The transition state largely correlates with the overall geometry change as related to the degree to which the dangling arm is or is not interacting with the cuprous-carbonyl upon Cu–C bond breakage. See below for further discussion.

Kinetics (k_{O2}; $\Delta H^{\ddagger}$, $\Delta S^{\ddagger}$) in THF of 1:1 Dioxygen Binding to ^{D}LCu^{I} following CO Photodissociation from ^{D}LCu^{I}-CO; D = Py, Im, NMe$_2$

The primary interaction (1:1) of O_2 with ^{Py}**LCu^{I}**, ^{Im}**LCu^{I}**, and ^{NMe2}**LCu^{I}** to form ^{D}**LCu^{II}-O$_2^-$** was monitored and measured in THF solvent through the "flash-and-trap" method.[15] The experiments were conducted in the presence of precisely determined concentrations of O_2 and CO within the temperature range of −55 °C to −85 °C on nanosecond and longer time scales. The ΔA spectra, Abs{[^{NMe2}LCu$^{I/II}$-X] – [^{NMe2}LCu^{I}-CO]} X = THF or O_2^-, representing the two separate O_2-binding processes (k_{fast}, k_{slow}) for formation of ^{NMe2}**LCu^{II}-O$_2^-$** are shown in Figures 6A-B; corresponding data for formation of ^{Im}**LCu^{II}-O$_2^-$** is given in the Supporting Information. As depicted in Scheme 6, the initial "fast" process (k_{fast}; Figure 6A) involves the competitive binding of both CO and O_2 with ^{D}**LCu^{I}**, either regenerating ^{D}**LCu^{I}-CO** or forming ^{D}**LCu^{II}-O$_2^-$**, thus, k_{fast} is a combination of two rate constants, k_{O2} and k_{CO}. Following generation of ^{D}**LCu^{II}-O$_2^-$**, since

$K_{CO} \gg K_{O2}$, CO subsequently displaces coordinated O_2 to reform the initial ^{D}**LCu^{I}-CO** species (k_{slow}). The latter values, k_{O2} (and K_{O2} and k_{-O2}) derived from k_{slow}, are tabulated here and used for discussion.

A full analysis of the O_2 binding kinetics and thermodynamics for formation of ^{Py}**LCu^{II}-O$_2^-$** was reported previously in THF solvent via the "flash-and-trap" method,[15] and in EtCN through stopped-flow UV-visible spectroscopy.[8] In the present work, analogous data for formation of ^{Im}**LCu^{II}-O$_2^-$** and ^{NMe2}**LCu^{II}-O$_2^-$** in THF are discussed and compared to that for ^{Py}**LCu^{II}-O$_2^-$**. Room temperature k_{O2} values were obtained by extrapolation from the activation parameters obtained at low temperatures where experimental data could be collected. All data here are also compared to those obtained by Schindler, Zuberbühler and coworkers on the closely related tripodal tetradentate ligand complex $[Cu^{I}(Me_6tren)]^+$ {tris(2-dimethylaminoethyl)amine},[62] see Table 3. In fact, very fast reactions with $k_{O2} > 10^7$ $M^{-1}s^{-1}$ at 298 K have only been observed and determined for the ^{D}**LCu^{I}** complexes described here, which includes the previously studied ^{Py}**LCu^{I}**, and $[Cu^{I}(Me_6tren)]^+$.[13-15]

Discussion

CO Equilibrium Binding and Thermodynamic Parameters (K_{CO}: ΔH°, ΔS°)

The K_{CO} values for formation of ^{D}**LCu^{I}-CO** increase as the $E_{1/2}$ values become more positive and the $^{4}\nu_{CO}$ values shift to higher energy (Table 1 and Table 2). In previous work that examined the CO binding properties of copper(I)-carbonyl adducts of the *R*-^{Py}L ligand series where only electronic effects are present, the opposite trend was observed; thus, a ligand having better donor properties led to enhanced CO binding.[59] This suggests that steric constraints or structural differences induced by changing the dangling "D" N-donor moiety of ^{D}**L** significantly affect the K_{CO} values in the present systems.

We suggest that the differences in ΔS° values or degree of disorder in the reaction are affiliated in part with the extent that the dangling "D" N-donor moiety is interacting with the final ^{D}**LCu^{I}-CO** adduct. For example, the Cu^{I}-CO adduct of the purely tridentate ^{Bz}**L** has the highest K_{CO} value of 5.6×10^4 M^{-1}. This clearly derives from ^{Bz}**LCu^{I}-CO** having the most favorable reaction enthalpy in the series, ΔH° = −46.0 kJ mol^{-1} K^{-1}, since the reaction is the most unfavored entropically, ΔS° = −63.6 kJ mol^{-1} K^{-1}. In more depth, formation of ^{Bz}**LCu^{I}-CO** is the most ordered reaction, meaning the benzyl D-group does not coordinate or donate any significant electron density to the cuprous center and also does not hinder coordination of CO to ^{Bz}**LCu^{I}**.

The K_{CO} values for CO binding to ^{Q}**LCu^{I}** and ^{TBP}**LCu^{I}** are the highest of the tetradentate ligands studied, 2.2×10^4 M^{-1} and 1.4×10^4 M^{-1} respectively. Based on their solution and solid state $^{4}\nu_{CO}$ values, the ligand-copper(I)-carbonyl complexes of both are tridentate in nature, consistent with the X-ray crystal structure of ^{TBP}**LCu^{I}-CO** (*vide supra*). However, in comparison to ^{Bz}**LCu^{I}-CO**, the coordination of CO to the cuprous ion of ^{Q}**LCu^{I}** and ^{TBP}**LCu^{I}** must be somewhat hindered by their bulky "D" N-donor groups (i.e., quinolyl or ^{t}Bu-pyridyl arms), resulting in their slightly lower K_{CO} values (Table 2).

At the low end of the range, reaction of ^{Im}**LCu^{I}** with CO results in the smallest K_{CO} value of 2.4×10^3 M^{-1} with the most favorable entropy, ΔS° = −40.6 kJ mol^{-1} K^{-1}. We suggest that the dangling imidazole is more interacting with the cuprous-carbonyl center resulting in increased disorder. The bond enthalpy for formation of ^{Im}**LCu^{I}-CO** is the highest (ΔH° = −31.4 kJ mol^{-1}), consistent with the weakest Cu–C bond of the series.

In comparison to the reaction of CO with ^{Py}**LCu^{I}**, the K_{CO} value of 1.2×10^4 M^{-1} is approximately five times higher as a result of the slightly lower thermodynamic values, ΔH°

= −35.9 kJ mol^{-1}, ΔS° = −42.6 kJ mol^{-1} K^{-1}.[59] Such small differences in the thermodynamic parameters, yet large effect on the equilibrium CO binding constant may suggest that the dangling pyridyl arm of ^{Py}**L** is less interacting with the cuprous ion than is the imidazolyl moiety of ^{Im}**L**.

By contrast, the equilibrium binding constant of K_{CO} = 5.0 × 10^3 M^{-1} for reaction of CO with ^{NMe2}**LCu^I** is lower. However, the highly negative ΔS° value of −62.5 kJ mol^{-1} K^{-1} is similar to that of ^{Bz}**LCu^I-CO** suggesting that the aliphatic dimethylamino arm is barely interacting if at all with the cuprous ion of ^{NMe2}**LCu^I** *in situ*. Such a characteristic is consistent with the absence of an observable $^5\nu_{CO}$ for ^{NMe2}**LCu^I-CO**.

CO Photodissociation and Rebinding Kinetics

The rate constant for formation of ^{D}**LCu^I-CO** (k_{CO}) appears to be controlled by the degree to which the dangling "D" arm interacts with the cuprous ion during Cu–C bond formation. This conclusion comes about from the observation that decreasing $^4\nu_{CO}$ frequencies for ^{D}**LCu^I-CO** along with decreased complex $E_{1/2}$ values for ^{D}**LCu^I**, which both indicate a better donor ligand, correlate with an increase in k_{CO} values (Table 1 and Table 2). For example, ^{Im}**LCu^I-CO** is comprised of the most electron-donating N-donor system for copper(I) due to the presence of the imidazolyl donor moiety and this complex gives the highest rate constant, k_{CO} = 2.8 × 10^9 M^{-1} s^{-1}. The corresponding activation parameters for formation of ^{Im}**LCu^I-CO**, ΔH‡ = 7.03 kJ mol^{-1} and ΔS‡ = −40.5 kJ mol^{-1} K^{-1}, are very similar to those measured for ^{Py}**LCu^I-CO**, suggesting little differences in the CO coordination dynamics. The coordination of CO to ^{Im}**LCu^I** is depicted in Scheme 2.

Consistent with the near equivalent $E_{1/2}$ values determined for ^{Im}**LCu^I** and ^{NMe2}**LCu^I**, ^{NMe2}**LCu^I-CO** has a similar CO rebinding rate of 2.5 × 10^9 M^{-1} s^{-1}. However, the ΔS‡ value affiliated with CO binding to ^{NMe2}**LCu^I** is much more positive than the ΔS° value suggesting that the course of reaction is more disordered as a result of the dangling or very weakly interacting donor moiety. Unlike for ^{Im}**LCu^I-CO** and ^{Py}**LCu^I-CO**, a five-coordinate carbonyl species is not structurally favorable for ^{NMe2}**LCu^I-CO**; in support of this supposition, note that only a $^4\nu_{CO}$ value was observed, *vide supra*. As a result, dissociation of the fourth ligand N-donor arm of ^{NMe2}**LCu^I** followed by subsequent CO rebinding likely involves significant structural changes resulting in a higher ΔS‡ value.

The parallel thermodynamic and activation parameters associated with CO binding to ^{Q}**LCu^I** (9.7 × 10^8 M^{-1} s^{-1}) and ^{TBP}**LCu^I** (5.2 × 10^8 M^{-1} s^{-1}) suggests that the mechanism of reaction is the same for both (Scheme 3). Such similarities are consistent with their analogous $^4\nu_{CO}$ values and identical $E_{1/2}$ values. Since solvent (THF) does not coordinate to ^{Q}**LCu^I** and ^{TBP}**LCu^I**, only the "D" N-donor must dissociate from the cuprous ion to form their respective ligand-copper(I)-carbonyl adducts.

Carbon monoxide rebinding to ^{Bz}**LCu^I**, where a fourth endogenous N-donor is not present, results in the lowest k_{CO} value of 5.0 × 10^8 M^{-1} s^{-1}; note that the Cu^{II}/Cu^I compound exhibits the most positive $E_{1/2}$ value. The negligible enthalpy (ΔH‡ = 0.74 kJ mol^{-1}) and highly negative entropy (ΔS‡ = −75.9 J mol^{-1} K^{-1}) of activation implies that the tridentate nature of ^{Bz}**L** minimizes geometric changes in the reaction of CO with ^{Bz}**LCu^I** and that the 'dangling' benzyl group does not hamper CO rebinding to the cuprous center. However, since the standard entropy (ΔS°) for formation of ^{Bz}**LCu^I-CO** is greater than the activation entropy (ΔS‡), it is possible that the CO molecule rebinds to the naked [Cu^I(^{Bz}L)]$^+$ species before THF transiently coordinates, resulting in a more ordered reaction and negligible enthalpy of activation (ΔH‡) as shown in Scheme 3.

Thermal ^{D}LCu^{I}-CO Dissociation Kinetics

As shown in Scheme 2 for CO dissociation from **^{Im}LCu^{I}-CO**, the dangling arm ligates to the copper(I) ion following CO dissociation. The negligible activation entropy ($\Delta S^{\ddagger} \sim 0$ J mol^{-1} K^{-1}) suggests that there is little overall geometry differences between the initial carbonylated complex and the transition state. Therefore, the increased donation offered by the slightly interacting imidazole in **^{Im}LCu^{I}-CO** results in an overall decrease in the structural changes as well as a decrease in the activation barrier to cleave the Cu–C bond. **^{Im}LCu^{I}-CO** has a k_{-CO} value of 1.1×10^{6} s^{-1} with a corresponding reaction enthalpy of $\Delta H^{\ddagger} = 38.5$ kJ mol^{-1}. Similar characteristics were exhibited by **^{Py}LCu^{I}-CO,**[59] **^{Q}LCu^{I}-CO**, and **^{TBP}LCu^{I}-CO** for CO dissociation, all with near zero $\Delta S^{\ddagger}$ values (Table 2).

Dissociation of CO from **^{NMe2}LCu^{I}-CO** is characterized by $\Delta S^{\ddagger} = 28$ J mol^{-1} K^{-1}, a more favorable value than is observed for any other in the series (Table 2). Thus, Cu–C bond cleavage involves considerable structural rearrangement and the high $\Delta S^{\ddagger}$ value implies an early transition state structurally similar to the terminal copper(I)-carbonyl species. Such a mechanism would require the dimethylamino donor arm of **^{NMe2}L** to be predominantly in the unbound state when the Cu–C bond is broken and further suggests that coordination of solvent occurs prior to or concomitant with CO release, see Scheme 4. As already stated, it is unfavorable for the hard dimethylamino arm to interact with the soft cuprous-carbonyl center, as evidenced or supported by a lack of observation of $^{5}\nu_{CO}$ for **^{NMe2}LCu^{I}-CO**.

Conversely, dissociation of CO from **^{Bz}LCu^{I}-CO** is accompanied by a strikingly unique unfavorable activation entropy of $\Delta S^{\ddagger} = -76$ J mol^{-1} K^{-1} that leads to the smallest k_{-CO} value (9.0×10^{3} s^{-1}) in the series. The almost identical $\Delta S^{\ddagger}$ values for the forward and reverse reaction of **^{Bz}LCu^{I}**/CO suggest that virtually no geometry change results and therefore the reaction is highly ordered, i.e. there is a late transition state.

Kinetics (k_{O2}; $\Delta H^{\ddagger}$, $\Delta S^{\ddagger}$) in THF of 1:1 Dioxygen Binding to ^{D}LCu^{I} following CO Photodissociation from ^{D}LCu^{I}-CO; D = Py, Im, NMe$_2$

An examination of activation parameters ($\Delta H^{\ddagger}$, $\Delta S^{\ddagger}$; Table 3) indicates there is a striking difference between those for formation of **^{Py}LCu^{II}-O$_2^-$** compared to the other two copper(II) η^1-superoxo complexes, **^{Im}LCu^{II}-O$_2^-$** and **^{NMe2}LCu^{II}-O$_2^-$**. The binding of O_2 to **^{Py}LCu^{I}** occurs with a relatively large and negative activation entropy (−45.1 J mol^{-1} K^{-1}, Table 3) indicating an associative reaction mechanism is involved.[15] This suggests O_2 binds prior to loss of the bound solvent molecule and then THF solvent de-ligates. Or, solvent may not even coordinate to the cuprous center, accounting for a simple (unhindered) association of dioxygen. As an example of the latter point, the tetradentate ligand-copper(I)-complex [Cu^{I}(Me$_6$-tren)]$^{+}$ does not coordinate an exogenously derived nitrile ligand.[14] As a result, an associative O_2 binding mechanism ($\Delta S^{\ddagger} = -52$ J mol^{-1} K^{-1}) resulted for formation of [Cu^{II}(Me$_6$-tren)(O$_2^-$)]$^{+}$ in EtCN, see Table 3. By extreme contrast, the positive activation entropies measured for **^{NMe2}LCu^{II}-O$_2^-$** ($\Delta S^{\ddagger} = 80.1$ J mol^{-1} K^{-1}) and **^{Im}LCu^{II}-O$_2^-$** ($\Delta S^{\ddagger} = 35.1$ J mol^{-1} K^{-1}) indicate that the O_2-binding reaction follows a dissociative mechanism where de-ligation of solvent (THF) occurs prior to O_2 binding. Throughout the remainder of the text, this latter reaction mechanism is referred to as a dissociative process, however, we note that a purely dissociative mechanism would result in first-order kinetics. Therefore, it is perhaps more appropriate to describe this process as a dissociative interchange reaction, in which bond breakage dominates over bond formation. More detailed explanation and analysis of the dioxygen binding mechanisms is given below.

As discussed earlier in the text, the structurally characterized cupric-chloride species **[^{NMe2}LCu^{II}(Cl)]**$^{+}$ has a square pyramidal geometry ($\tau = 0.26$),[62] different than the trigonal bipyramidal structures exhibited by **[^{Py}LCu^{II}(Cl)]**$^{+}$ ($\tau = 1.00$),[88] **[^{Py}LCu^{II}(CH$_3$CN)]$^{2+}$** ($\tau =$

0.96),[67] and **[^{Im}LCu^{II}(CH$_3$CN)]$^{2+}$** (τ = 0.86)[65,86] Also, the complementary ligand-copper(I)-CH_3CN structures of the three aforementioned species **^{D}LCu^{I}** have analogous trigonal bipyramidal geometries. Therefore, based on the assumption that the cupric-superoxo species are analogous in structure to their X-ray crystallographically characterized copper(II) adducts, the structural rearrangement that results upon redox changes in the **^{NMe2}L** ligand system would be much greater. Consistent with this supposition is the observed highly positive activation entropy $\Delta S^{\ddagger}$ = 80.1 kJ mol^{-1} for the reaction of O_2 with **^{NMe2}LCu^{I}**. Also, the overall redox process, i.e. O_2-binding, results in a higher enthalpy of activation of $\Delta H^{\ddagger}$ = 32.1 kJ mol^{-1}. The more favorable activation enthalpy for O_2 binding to **^{Im}LCu^{I}** ($\Delta H^{\ddagger}$ = 23.4 kJ mol^{-1}) and less favorable $\Delta S^{\ddagger}$ (35.1 kJ mol^{-1}) in comparison to **^{NMe2}LCu^{I}** is consistent with a smaller geometry change with copper redox state due to O_2-binding.

Solvent dependence (EtCN vs THF) of 1:1 Copper-Dioxygen Adducts

The dynamics of the O_2 binding reaction of **^{Py}LCu^{I}** are largely influenced by solvent medium based on the analogous O_2 binding data collected through the "flash-and-trap" method in THF[15] and stopped-flow UV-visible spectroscopy in EtCN,[8] see Table 3. The entropy of activation ($\Delta S^{\ddagger}$) for formation of **^{Py}LCu^{II}-O$_2^-$** in EtCN ($\Delta S^{\ddagger}$ = 10 J mol^{-1} K^{-1}) versus THF ($\Delta S^{\ddagger}$ = −45.1 J mol^{-1} K^{-1}) indicates that O_2 binding to **^{Py}LCu^{I}** follows a dissociative versus associative pathway, respectively, depending on the solvent. To observe such a solvent effect is not an unreasonable expectation since nitrile solvents are strong Lewis bases and soft donors, therefore strong ligands for copper(I) ions. In some cases, nitrile solvents severely inhibit binding of dioxygen such as in the reaction of O_2 with **^{Bz}LCu^{I}**, where EtCN solvent prevents formation of the commonly observed O_2 adduct, characterized as a dicopper(III) bis-μ-oxo species in less coordinating solvents (THF, acetone, toluene).[60]

Previously, Schindler and coworkers attempted to time-resolve the formation of the cupric superoxo species **^{NMe2}LCu^{II}-O$_2^-$**.[62] However, the formation was too fast to be measured by stopped-flow UV-visible spectroscopy, even in EtCN (coordinating solvent) at 183 K. Similarly, we have unsuccessfully attempted to measure the formation of **^{Im}LCu^{II}-O$_2^-$** by stopped-flow methods in EtCN.[65] Conversely, the k_{O2} value for O_2 binding to **^{Py}LCu^{I}** in EtCN was easily measured (Table 3). These comparisons suggest that like the k_{O2} measurements in THF, a much higher k_{O2} value in EtCN is expected for formation of **^{NMe2}LCu^{II}-O$_2^-$** and **^{Im}LCu^{II}-O$_2^-$** compared to **^{Py}LCu^{II}-O$_2^-$**. Such measurements for formation of **^{NMe2}LCu^{II}-O$_2^-$** and **^{Im}LCu^{II}-O$_2^-$** in EtCN were not carried out, but the values of k_{O2} reported here in THF through the present "flash-and-trap" experiment, indeed are very large (> 6.9 × 10^7 M^{-1} s^{-1} at 193 K; see Table 3), above the limit of stopped-flow UV-visible spectroscopic methods (ms timescale).

THF is usually considered a weakly coordinating solvent for ligand-copper-species and has even been described as a non-coordinating solvent. However, THF contains an electron pair centered on the oxygen-atom potentially capable of binding to copper(I) or any Lewis acid. A series of ligand-copper(II)-peroxo complexes utilizing the tridentate ligand R-MePY2 {bis[2-(2-pyridyl)ethyl]methylamine; R = Cl-, H-, MeO-, NMe_2-} with 4-pyridyl substituents were previously reported to efficiently oxidize THF to 2-hydroxy tetrahydrofuran (THF-OH).[85] Substrate (THF) oxidation was proposed as an "inner-sphere oxidation" because of a likely pre-equilibrium step involving THF-binding to the copper-dioxygen adduct.[89] Also, in a detailed study conducted by Tolman and coworkers on the mechanism of formation for the β-diketiminate Cu^{III}-η^2-O$_2^{2-}$ adduct, an associative oxygenation pathway (Scheme 7) involving THF coordination (pathway B) was proposed based on comparisons to the same reaction in THF/MeCN mixtures (pathway A).[13]

Complementary theoretical calculations led to a proposed transition state that involved dioxygen and solvent bound to copper simultaneously, either THF or MeCN accordingly.

Proposed Mechanisms for O_2-Binding to the ^{D}LCu^{I} Complexes (D = NMe_2, Im, Py)

In the present work and as described above, positive $\Delta S^{\ddagger}$ values were measured for O_2 binding to ^{Im}**LCu^{I}** ($\Delta S^{\ddagger}$ = 35.1 J mol^{-1} K^{-1}) and ^{NMe2}**LCu^{I}** ($\Delta S^{\ddagger}$ = 80.1 J mol^{-1} K^{-1}) in THF solvent, to the first approximation similar to that found for ^{Py}**LCu^{I}** in EtCN, but very different to that for ^{Py}**LCu^{I}** in THF (and [Cu^{I}(Me_6tren)]$^{+}$ in EtCN), see Table 3. Such a drastic difference in the O_2-binding mechanism depending on the variable N-donor moiety of ^{D}**L** is surprising. We suggest changes in the electron distribution and/or coordination variations within the species upon O_2 ligation to Cu^{I} are responsible and it is not simply related to the order in which O_2 or solvent coordinate. More specifically, the transition state differences may be largely based on whether or not Cu^{I} → O_2 electron transfer (*et*) occurs before or after solvent dissociation with the coordination of O_2 always being the initial step.

As shown in Scheme 8, the negative k_{O2} affiliated $\Delta S^{\ddagger}$ value (associative mechanism) for ^{Py}**LCu^{II}-O_2^{-}** in THF suggests a late transition state in which *et* occurs before or concomitant with solvent release. Conversely, the positive k_{O2} affiliated $\Delta S^{\ddagger}$ value (dissociative mechanism) for O_2 binding to ^{Im}**LCu^{I}** in THF, ^{NMe2}**LCu^{I}** in THF, and ^{Py}**LCu^{I}** in EtCN, suggests an early transition state in which *et* can occur only after solvent is released, see Scheme 8. Note that a computational analysis of the proposed mechanism has not been conducted and therefore the proposed internal electron density distributions or solvent positioning (ligated or not) cannot be conclusively supported. However, the similar dissociative processes for formation of the square pyramidal ^{NMe2}**LCu^{II}-O_2^{-}** species in THF and the trigonal bipyramidal ^{Im}**LCu^{II}-O_2^{-}** and ^{Py}**LCu^{II}-O_2^{-}** species in THF and EtCN (respectively) again points out that the reaction mechanism is not solely dependent on geometry or solvent medium, but rather the degree of solvent and/or O_2-fragment interaction, i.e. electronic distribution within a given species.

Smirnov and Roth have proposed a two-step, inner-sphere electron-transfer mechanism for the oxidation of $O_2^{\bullet-}$ to O_2 by the copper(II)-complexes of ^{Py}**L** and TEPA (tris(2-pyridylethyl)amine) in DMF/THF mixtures (DMF = dimethylformamide).[90] Based on low-temperature stopped-flow kinetic experiments and competitive $^{18}O_2$ isotope effects, a pre-equilibrium step with formation of a Cu-O_2 species was suggested to form prior to O_2 release, see Scheme 9. Formal oxidation states were not emphasized (Cu^{II}-O_2^{-} versus Cu^{I}-O_2) for the intermediate species; therefore an electrostatic versus covalent Cu–O_2 interaction was not designated. However, the release of O_2 was designated as the rate determining step which would complete the overall *et* process, i.e. reduction of the copper(II) ion. Formation of a pre-equilibrium complex is analogous to our proposal of a pre-electron transfer intermediate step upon formation of ^{D}**LCu^{II}-O_2^{-}** (Scheme 9).

Temperature dependence (193 K vs. 298 K) of equilibrium O_2 binding constants (K_{O2}; ΔH°, ΔS°) and dissociation rates (k_{-O2}; $\Delta H^{\ddagger}$, $\Delta S^{\ddagger}$)

Dissociation of O_2 from ^{D}**LCu^{II}-O_2^{-}** has an early transition state (+$\Delta S^{\ddagger}$) for all species studied that involves the transfer of an electron (*et*) from $O_2^{\bullet-}$ to copper(II) followed by coordination of solvent (THF) and concomitant release of O_2. This Cu-O_2 bond breakage process is depicted for ^{Im}**LCu^{II}-O_2^{-}** in Scheme 10. The k_{-O2} activation parameters corresponding to ^{Im}**LCu^{II}-O_2^{-}** are almost the same as those for ^{NMe2}**LCu^{II}-O_2^{-}** suggesting the same O_2 release mechanism. However, for O_2 dissociation from ^{Py}**LCu^{II}-O_2^{-}**, the corresponding activation parameters (Table 3) are of slightly higher values than the aforementioned species suggesting a larger geometric change upon dioxygen loss.

The O_2 binding constants (K_{O2}) for all ^{D}**LCu^{II}-O$_2^-$** complexes are of approximately the same magnitude (10^5 M^{-1}) at 193 K, overall favoring formation of the cupric-superoxo species. As expected, the equilibrium shifts more towards formation of the solvento species at 298 K. The K_{O2} values clearly show the solvent effect where as compared to THF, EtCN significantly inhibits O_2 binding to ^{Py}**LCu^{I}**. However, Me_6TREN is a more Lewis basic ligand than is ^{Py}**L** such that O_2 binding to $[Cu^{I}(Me_6tren)]^+$ seems unaffected.

Summary of 1:1 Cu/CO and Cu/O_2 binding to ^{D}LCu^{I} and Related Cu/O_2 = 2:1 Complexes

In the present study, CO, as a redox-inactive O_2-surrogate, was examined in its interactions with ligand-copper(I)-complexes (^{D}**LCu^{I}**). Data obtained concerning the CO binding kinetics and thermodynamics in THF were compared to those for 1:1 O_2 binding to ^{Py}**LCu^{I}**, ^{Im}**LCu^{I}**, and ^{NMe2}**LCu^{I}**, where end-on (η^1) coordination occurs. The formation of 1:1 Cu/O_2 adducts were not observed for ^{Q}**LCu^{I}**, ^{TBP}**LCu^{I}**, and ^{Bz}**LCu^{I}** under the same solution reaction conditions by laser flash photolysis of the CO adducts.[91] Since these cuprous complexes in fact do react with dioxygen to form 2:1 Cu/O_2 species under steady state conditions,[60,63,64] it is likely that primary 1:1 Cu/O_2 binding does not compete kinetically (e.g., $\Delta_{absorbance}$ is too small) under the conditions employed, i.e., those used for all of the complexes examined in these studies.

In our previous reports,[15,59] the CO and O_2 binding kinetics of ^{Py}**LCu^{I}** in THF solvent were detailed, with one finding being that $k_{CO} \approx k_{O2}$ (Table 2). A look at the highlighted portion of Table 4, with data added in from the present study on ^{Im}**LCu^{I}** and ^{NMe2}**LCu^{I}** (i.e., with one altered N-donor arm), gives the impression that these latter complexes have a very similar behavior. However, a significant finding in this report (Tables 3 and 4) is that there is a major change in the mechanism of O_2-binding to ^{Im}**LCu^{I}** and ^{NMe2}**LCu^{I}** in THF; *the ligand binding occurs via dissociative rather than associative processes*. Recall that the dissociative mechanism *does occur* for both CO and O_2 binding to ^{Py}**LCu^{I}** in the strong competing solvent EtCN. Electron-transfer (*et*) from copper(I) to O_2 seems the only factor possible to explain a change in mechanism. The CO binding behavior to the reduced copper(I) species for the ^{D}**L** series is essentially the same (Tables 1, 2). The (electrochemical study) derived $E_{1/2}$ values for ^{Im}**LCu^{I}** and ^{NMe2}**LCu^{I}** are the same, but more negative than that for ^{Py}**LCu^{I}**, however the coordination geometries of the copper(II) complexes of ^{Im}**L** (~ ^{Py}**L**) and ^{NMe2}**L** are different (*vide supra*). Thus, we conclude that the *et* properties/kinetics of the O_2-interaction somehow leads to the change in mechanism observed. Solvent release is initiated by O_2-interaction with copper(I) (i.e., we suggest a Cu^{I}-O_2 transient forms) *prior* to *et* (Scheme 8) giving the observed ^{D}**LCu^{II}-O$_2^-$** product. To summarize in other words, the reaction mechanism is governed by the order that *et* from copper(I) to O_2 occurs; for ^{Py}**L**, *et* occurs before solvent is released, perhaps outer-sphere, but not so for ^{Im}**L** or ^{NMe2}**L**. For ^{Im}**L** and ^{NMe2}**L**, a dissociative interchange mechanism (*vide supra*) may be an appropriate description in which bond breaking (Cu^{I}-solv → Cu^{I} + solv) dominates over bond formation and *et* ($Cu^{I} + O_2 \rightarrow Cu^{II}$-$O_2^-$).

For all ligand-copper-complexes studied, K_{CO} is much larger than K_{O2} primarily as a result of the lower CO dissociation rate constant ($k_{-CO} < k_{-O2}$). Breakage of the Cu-O_2 bond is more favorable than Cu-CO bond breakage even though the former involves an *et* step. The high k_{-O2} values are a result of the highly favorable $\Delta S^{\ddagger}$ value attributed to a late transition state (which leads to O_2-release) and the structural rearrangement that occurs upon redox changes.

As emphasized, the copper(II)-η^1-superoxo species generated from ^{Py}**LCu^{I}**, ^{Im}**LCu^{I}**, and ^{NMe2}**LCu^{I}**, are spectroscopically very similar. In fact, spectroscopically (and therefore structurally) similar Cu/O_2 = 2:1 adducts also form, dicopper(II)-μ-1,2-(*end-on*)-peroxo species $[\{(^{D}L)Cu^{II}\}_2(O_2^{2-})]^{2+}$ analogous to the well characterized case for ^{Py}**L** (Scheme

11).[8,61,62,65] However, the conditions (i.e. temperature) under which the $[\{(^{D}L)Cu^{II}\}_2(O_2^{2-})]^{2+}$ complexes are observed, and/or their relative stability, varies significantly. Thus, reaction dynamics, i.e., kinetics and thermodynamics, governing each reaction step likely vary significantly, as observed in the present study on the Cu/O_2 = 1:1 adducts. For example, the peroxo species of ^{Im}**L** (Figure 7A) can only be observed at −128 °C in 2-methyl tetrahydrofuran (MeTHF).[65] In THF at −80 °C, a $Cu\text{-}O_2$ intermediate is not observed.[65] Quite differently, formation of ^{Py}**LCu^{II}-O$_2^-$** can be detected on the bench-top in MeTHF at −128 °C before complete conversion to the peroxo species (Figure 7B), which is stable for weeks at −80°C in THF.[61] Interestingly, for ^{NMe2}**LCu^{I}** + O_2, a new as yet uncharacterized species is detected in MeTHF at −128 °C in addition to the peroxo adduct (Figure 7C).[76] The new UV-vis feature(s) may suggest a different type or additional intermediate forms on the pathway to produce $[\{(^{NMe2}L)Cu^{II}\}_2(O_2^{2-})]^{2+}$; further studies are required.

Comparison to natural copper and heme systems

The kinetics and thermodynamics of CO and O_2 binding to the ligand-copper(I)-complexes (**^{D}LCu^{I}**) reported here are in line with studies carried out on natural and synthetic heme systems (Table 4). As said, carbon monoxide coordinates to the cuprous center (**^{D}LCu^{I}**) with a higher affinity than that of O_2 ($K_{CO} > K_{O2}$), allowing for extension of the "flash-and-trap" experiment as inspired by extensive studies on a variety of heme systems. Furthermore, like our synthetic species, K_{CO} is much higher than K_{O2} for the porphyrinate systems as a result of the lower CO dissociation rate ($k_{-CO} < k_{-O2}$); $Cu\text{-}O_2$ bond breakage is more favorable than breakage of the Cu-CO bond. The bimolecular rate constants for the copper complexes (k_{CO} and k_{O2}) are much higher than typically exhibited by heme systems and the equilibrium binding constants are much lower. Therefore, the trends observed here are in line with conclusions drawn concerning gaseous small molecule binding at the active site of the heme-copper heterobimetallic enzyme cytochrome *c* oxidase (C*c*O) (*vide supra*; see Introduction). In C*c*O, where one can imagine some competition for gases by both the heme and copper, CO coordinates to the Cu^{I}_{B} site before thermally transferring to the Fe^{II}-$heme_{a3}$ site (Figure 1). We have previously constructed a model binucleating iron and copper containing ligand system as well as 1:1 heme/copper component systems that demonstrate this CO migration phenomenon, and most recently have additionally examined NO transfer from iron-to-copper in the latter 1:1 component system.[22,25]

The interaction of CO and O_2 with hemocyanins (Hc) has also been extensively studied and the characteristics are unlike hemes. For Hc, lower equilibrium CO binding constants in comparison to O_2 ($K_{O2} > K_{CO}$) has been attributed to the higher rate of CO dissociation in comparison to that for O_2 ($k_{-CO} > k_{-O2}$) see Table 4. This behavior most likely occurs because both copper(II) centers are involved in O_2-binding and release, whereas only one copper center binds CO; more structural rearrangements must occur in the release of O_2. Conversely, the high O_2 association rates (k_{O2}) are a result of the 2:1 Cu/O_2 binding nature of the binuclear copper protein, a characteristic that is not exhibited upon CO binding (1:1 Cu/CO binding), *vide supra*.

As stated in the Introduction, an experiment such as the flash-and-trap experiment cannot be utilized for the binuclear copper proteins because $K_{O2} > K_{CO}$. Laser flash photolysis has been used by Hirota *et al*. to examine O_2 binding by tyrosinase (Tyr) from *Streptomyces antibioticus*.[44] Following O_2-photoejection from oxy-Tyr to form deoxy-Tyr, reformation of the starting dicopper(II)-μ-η^2:η^2-peroxo species was observed while an initial 1:1 Cu/O_2 adduct was not detected. In a more recent study, Hirota, Bubacco, and coworkers reported thermodynamic data for oxygenation of Hc to form the dicopper(II)-(*side-on*)-peroxo species.[45] Interestingly, the values were comparable to the superoxo model compounds measured here, suggesting that formation of the 1:1 adduct is the rate-determining step and

that oxyHc is easily produced through a nearly simultaneous two *et* step. This experimental finding fits with Solomon and coworkers' prior computational studies on the O_2-binding process that occurs in Hc.[92]

Summary and Conclusions

In the present report, we have detailed the kinetics, thermodynamics, and coordination dynamics of 1:1 Cu^I/CO and Cu^I/O_2 binding within tetradentate ligand-copper(I)-complexes with analogous coordination frameworks (Chart 2). The major findings are:

1. In the ligand-copper(I) carbonyl complexes ($^{\mathbf{D}}\mathbf{LCu^I}$), the variable N-donor arm of the synthetic ligand is dangling; all species possess the same four-coordinate core structure in solution where the cuprous ion binds to the bispicolylamine (PY1) tridentate chelate along with the CO molecule.
2. The fast kinetics of CO binding are measurably influenced by the exact nature of that uncoordinated donor arm. With change in ligand where K_{CO} increases, k_{CO} and k_{-CO} decrease; k_{-CO} decreases more substantially because the dangling donor ligand partially interacts (but to different extents) before it fully coordinates with the Cu(I) ion as CO dissociates.
3. In previous studies where the exact same PY1 ligand framework was present but with more electron releasing 4-pyridyl substituents, K_{CO} increased, as well as k_{CO}, very different from what was found here. In other words, ligand electronic variations previously led to the standard expected results, but here, (small) changes in the identity of D (the fourth donor, 3rd ligand arm, Chart 1) led to a change in the relationship of K_{CO} to k_{CO}.
4. Using nanosecond laser flash photolysis to initiate gas (CO, O_2) reactions with copper(I) complexes, the unique finding of an extremely large rate constant for O_2 binding, as previously described for $^{\mathbf{Py}}\mathbf{LCu^I}$, is shown to be a general phenomenon amongst D-PY1 ligand copper(I) complexes. Further, as seen before, k_{O2} and k_{CO} values are quite similar to each other.
5. Changing one donor arm N-ligand from pyridyl to imidazolyl or to dimethylamino results in a change in the mechanism of O_2-binding to the respective copper(I) complexes, associative for $^{\mathbf{Py}}\mathbf{LCu^I}$ but dissociative for $^{\mathbf{Im}}\mathbf{LCu^I}$ and $^{\mathbf{NMe_2}}\mathbf{LCu^I}$. We attribute this to aspects of the timing of *et* from copper(I) to O_2 as this molecule coordinates, in relation to the dissociation of the bound solvent molecule THF. Based on our other experiments, the change in mechanism is not simply related to a change in the $^{\mathbf{D}}\mathbf{LCu^{II/I}}$ structures or the order that O_2/THF coordinate.
6. The work discussed here establishes transient absorbance laser flash photolysis as an invaluable tool for determining fast small molecule (CO *and* O_2) binding kinetics and thermodynamics to synthetic copper complexes such as $^{\mathbf{D}}\mathbf{LCu^I}$. Further, the ability to combine this utility with variable low-temperature control has enabled us to fully characterize 1:1 binding of O_2 to $^{\mathbf{Im}}\mathbf{LCu^I}$ and $^{\mathbf{NMe_2}}\mathbf{LCu^I}$, which was previously unobtainable with other relatively fast physical methods such as low-temperature stopped flow kinetics/spectroscopy.

Overall the results further support the general finding that subtle changes in coordination environment, as occurs over time through evolution in nature or through controlled ligand design in synthetic systems, can dictate the observed chemistry in terms of reaction kinetics, structure and reactivity, and thus function. Many mononuclear and binuclear copper proteins exist that have an active site ligation of three imidazolyl donors per copper center, yet have very different functions, such as dioxygen transport in hemocyanin (Hc), dioxygen

activation and phenol *o*-hydroxylation in tyrosinase (Tyr), electron-transfer (*et*) at the Cu_H site in peptidylglycine α-hydroxylating monooxygenase (PHM) and/or dopamine β-monooxygenase, or O_2-binding (and/or *et*) at Cu_B in cytochrome *c* oxidases (C*c*O), see Introduction. Therefore, by gaining a deeper understanding of how the coordination environment and/or subtle changes in the surroundings influence the reactivity and/or binding properties of the copper center may help in understanding protein active site ligand dynamics. Such information may also provide insight into secondary coordination sphere contributions that account for N_3Cu^I active site functional differences.

Supplementary Material

Refer to Web version on PubMed Central for supplementary material.

Acknowledgments

We are grateful to the National Institutes of Health (K.D.K., NIH GM28962; G.J.M., NSF CHE0911558) for support of this research. We also acknowledge Drs. Amy A. Narducci Sarjeant and Maxime A. Siegler for relevant X-ray structural determination.

References

1. Kim E, Chufan EE, Kamaraj K, Karlin KD. chem Rev. 2004; 104:1077–1133. [PubMed: 14871150]
2. Wasser IM, de Vries S, Moenne-Loccoz P, Schroder I, Karlin KD. Chem Rev. 2002; 102:1201–1234. [PubMed: 11942794]
3. Lucas HR, Karlin KD. Met Ions Life Sci. 2009; 6:295–362. [PubMed: 20877799]
4. Lewis EA, Tolman WB. Chem Rev. 2004; 104:1047–1076. [PubMed: 14871149]
5. Mirica LM, Ottenwaelder X, Stack TDP. Chem Rev. 2004; 104:1013–1045. [PubMed: 14871148]
6. Solomon EI, Szilagyi RK, George SD, Basumallick L. Chem Rev. 2004; 104:419–458. [PubMed: 14871131]
7. Woertink JS, Smeets PJ, Groothaert MH, Vance MA, Sels BF, Schoonheydt RA, Solomon EI. Proc Nat Acad Sci. 2009; 106:18908–18913. [PubMed: 19864626]
8. Zhang CX, Kaderli S, Costas M, Kim E, Neuhold YM, Karlin KD, Zuberbuhler AD. Inorg Chem. 2003; 42:1807–1824. [PubMed: 12639113]
9. Himes RA, Karlin KD. Curr Opin Chem Biol. 2009; 13:119–131. [PubMed: 19286415]
10. Maiti D, Lee DH, Gaoutchenova K, Wurtele C, Holthausen MC, Sarjeant AAN, Sundermeyer J, Schindler S, Karlin KD. Angew Chem Int Ed. 2008; 47:82–85.
11. Würtele C, Gaoutchenova E, Harms K, Holthausen MC, Sundermeyer J, Schindler S. Angew Chem Int Ed. 2006; 45:3867–3869.
12. Fujisawa K, Tanaka M, Morooka Y, Kitajima N. J Am Chem Soc. 1994; 116:12079–12080.
13. Aboelella NW, Kryatov SV, Gherman BF, Brennessel WW, Young VG, Sarangi R, Rybak-Akimova EV, Hodgson KO, Hedman B, Solomon EI, Cramer CJ, Tolman WB. J Am Chem Soc. 2004; 126:16896–16911. For comparison, $k_{O2} \sim 10^4\ M^{-1}\ s^{-1}$ for βDkCu^I. [PubMed: 15612729]
14. Weitzer M, Schindler S, Brehm G, Schneider S, Hormann E, Jung B, Kaderli S, Zuberbuhler AD. Inorg Chem. 2003; 42:1800–1806. [PubMed: 12639112]
15. Fry HC, Scaltrito DV, Karlin KD, Meyer GJ. J Am Chem Soc. 2003; 125:11866–11871. [PubMed: 14505408]
16. Itoh S, Fukuzumi S. Acc Chem Res. 2007; 40:592–600. [PubMed: 17461541]
17. Itoh S. Curr Opin Chem Biol. 2006; 10:115–122. [PubMed: 16504568]
18. Prigge ST, Eipper BA, Mains RE, Amzel LM. Science. 2004; 304:864–867. [PubMed: 15131304]
19. Humphreys KJ, Mirica LM, Wang Y, Klinman JP. J Am Chem Soc. 2009; 131:4657–4663. [PubMed: 19290629]
20. Kitagawa T, Ogura T. Prog Inorg Chem. 1997; 45:431–479.
21. Larsen RW, Mikšovská J. Coord Chem Rev. 2007; 251:1101–1127.

22. Fry HC, Cohen AD, Toscano JP, Meyer GJ, Karlin KD. J Am Chem Soc. 2005; 127:6225–6230. [PubMed: 15853327]
23. Fry HC, Hoertz PG, Wasser IM, Karlin KD, Meyer GJ. J Am Chem Soc. 2004; 126:16712–16713. [PubMed: 15612695]
24. Fry HC, Lucas HR, Zakharov LN, Rheingold AL, Meyer GJ, Karlin KD. Inorg Chim Acta. 2008; 361:1100–1115.
25. Lucas HR, Meyer GJ, Karlin KD. J Am Chem Soc. 2009; 131:13924–5. [PubMed: 19736941]
26. Vos MH. Biochim Biophys Acta. 2008; 1777:15–31. [PubMed: 17996720]
27. Dyer RB, Peterson KA, Stoutland PO, Woodruff WH. J Am Chem Soc. 1991; 113:6276–6277.
28. Spiro TG, Wasbotten IH. J Inorg Biochem. 2005; 99:34–44. [PubMed: 15598489]
29. Rousseau DL, Han S. Method Enzymol. 2002; 354:351–368.
30. Ionascu D, Gruia F, Ye X, Yu AC, Rosca F, Beck C, Demidov A, Olson JS, Champion PM. J Am Chem Soc. 2005; 127:16921–16934. [PubMed: 16316238]
31. Kapetanaki SM, Field SJ, Hughes RJL, Watmough NJ, Liebl U, Vos MH. Biochim Biophys Acta. 2008; 1777:919–924. [PubMed: 18420024]
32. Gibson QH, Greenwood C. Biochem J. 1963; 86:541–&. [PubMed: 13947736]
33. Greenwood C, Gibson QH. J Biol Chem. 1967; 242:1782–&. [PubMed: 4290651]
34. Einarsdottir O, Szundi I. Biochim Biophys Acta. 2004; 1655:263–73. [PubMed: 15100041]
35. Szundi I, Rose MJ, Sen I, Eroy-Reveles AA, Mascharak PK, Einarsdottir O. Photochem Photobiol. 2006; 82:1377–84. [PubMed: 17421079]
36. Soldatova AV, Ibrahim M, Olson JS, Czernuszewicz RS, Spiro TG. J Am Chem Soc. 132:4614–25. [PubMed: 20218710]
37. Birukou I, Schweers RL, Olson JS. J Biol Chem. 2010; 285:8840–8854. [PubMed: 20080971]
38. Ohta K, Muramoto K, Shinzawa-Itoh K, Yamashita E, Yoshikawa S, Tsukihara T. Acta Crystallogr F. 2010; 66:251–253.
39. Babcock GT, Floris R, Nilsson T, Pressler M, Varotsis C, Vollenbroek E. Inorg Chim Acta. 1996; 243:345–353.
40. Oliveberg M, Malmstrom BG. Biochemistry. 1992; 31:3560–3563. [PubMed: 1314642]
41. Muramoto K, Ohta K, Shinzawa-Itoh K, Kanda K, Taniguchi M, Nabekura H, Yamashita E, Tsukihara T, Yoshikawa S. Proc Nat Acad Sci. 2010; 107:7740–5. [PubMed: 20385840]
42. Magnus KA, Hazes B, Tonthat H, Bonaventura C, Bonaventura J, Hol WGJ. Proteins. 1994; 19:302–309. [PubMed: 7984626]
43. Solomon EI, Tuczek F, Root DE, Brown CA. Chem Rev. 1994; 94:827–856.
44. Hirota S, Kawahara T, Lonardi E, de Waal E, Funasaki N, Canters GW. J Am Chem Soc. 2005; 127:17966–17967. [PubMed: 16366523]
45. Hirota S, Kawahara T, Beltramini M, Di Muro P, Magliozzo RS, Peisach J, Powers LS, Tanaka N, Nagao S, Bubacco L. J Biol Chem. 2008; 283:31941–31948. [PubMed: 18725416]
46. Floyd JS, Haralampus-Grynaviski N, Ye T, Zheng B, Simon JD, Edington MD. J Phys Chem B. 2001; 105:1478–1483.
47. Guëll M, Siegbahn PEM. J Biol Inorg Chem. 2007; 12:1251–1264. [PubMed: 17891425]
48. Jaron S, Blackburn NJ. Biochemistry. 1999; 38:15086–15096. [PubMed: 10563791]
49. Jaron S, Mains RE, Eipper BA, Blackburn NJ. Biochemistry. 2002; 41:13274–13282. [PubMed: 12403629]
50. Wilmot CM, Hajdu J, McPherson MJ, Knowles PF, Phillips SEV. Science. 1999; 286:1724–1728. [PubMed: 10576737]
51. Mukherjee A, Smirnov VV, Lanci MP, Brown DE, Shepard EM, Dooley DM, Roth JP. J Am Chem Soc. 2008; 130:9459–9473. [PubMed: 18582059]
52. Shepard EM, Okonski KM, Dooley DM. Biochemistry. 2008; 47:13907–13920. [PubMed: 19053231]
53. Hirota S, Iwamoto T, Tanizawa K, Adachi O, Yamauchi O. Biochemistry. 1999; 38:14256–14263. [PubMed: 10571999]

54. Alben JO, Moh PP, Fiamingo FG, Altschuld RA. Proc Nat Acad Sci. 1981; 78:234–237. [PubMed: 6264435]
55. Hill J, Goswitz VC, Calhoun M, Garciahorsman JA, Lemieux L, Alben JO, Gennis RB. Biochemistry. 1992; 31:11435–11440. [PubMed: 1332759]
56. Einarsdottir O, Killough PM, Fee JA, Woodruff WH. J Biol Chem. 1989; 264:2405–2408. [PubMed: 2536707]
57. Zhang HM, Boulanger MJ, Mauk AG, Murphy MEP. J Phys Chem B. 2000; 104:10738–10742.
58. Fager LY, Alben JO. Biochemistry. 1972; 11:4786–4792. [PubMed: 4655254]
59. Fry HC, Lucas HR, Sarjeant AAN, Karlin KD, Meyer GJ. Inorg Chem. 2008; 47:241–256. [PubMed: 18052158]
60. Lucas HR, Li L, Sarjeant AAN, Vance MA, Solomon EI, Karlin KD. J Am Chem Soc. 2009; 131:3230–3245. [PubMed: 19216527]
61. Tyeklár Z, Jacobson RR, Wei N, Murthy NN, Zubieta J, Karlin KD. J Am Chem Soc. 1993; 115:2677–2689.
62. Weitzer M, Schatz M, Hampel F, Heinemann FW, Schindler S. J Chem Soc, Dalton Trans. 2002:686–694.
63. Wei N, Murthy NN, Chen Q, Zubieta J, Karlin KD. Inorg Chem. 1994; 33:1953–1965.
64. Maiti D, Lucas HR, Sarjeant AAN, Karlin KD. J Am Chem Soc. 2007; 129:6998–6999. [PubMed: 17497785]
65. Lee Y, Park GY, Lucas HR, Vajda PL, Kamaraj K, Vance MA, Milligan AE, Woertink JS, Siegler MA, Sarjeant AAN, Zakharov LN, Rheingold AL, Solomon EI, Karlin KD. Inorg Chem. 2009; 48:11297–11309. [PubMed: 19886646]
66. Liang HC, Kim E, Incarvito CD, Rheingold AL, Karlin KD. Inorg Chem. 2002; 41:2209–2212. [PubMed: 11952376]
67. Lim BS, Holm RH. Inorg Chem. 1998; 37:4898–4908. [PubMed: 11670655]
68. See Supporting Information.
69. Pasquali M, Marini G, Floriani C, Gaetanimanfredotti A, Guastini C. Inorg Chem. 1980; 19:2525–2531.
70. Kitajima N, Fujisawa K, Fujimoto C, Morooka Y, Hashimoto S, Kitagawa T, Toriumi K, Tatsumi K, Nakamura A. J Am Chem Soc. 1992; 114:1277–1291.
71. Karlin KD, Tyeklar Z, Farooq A, Haka MS, Ghosh P, Cruse RW, Gultneh Y, Hayes JC, Toscano PJ, Zubieta J. Inorg Chem. 1992; 31:1436–1451.
72. Ardizzoia GA, Beccalli EM, Lamonica G, Masciocchi N, Moret M. Inorg Chem. 1992; 31:2706–2711.
73. Imai S, Fujisawa K, Kobayashi T, Shirasawa N, Fujii H, Yoshimura T, Kitajima N, Moro-oka Y. Inorg Chem. 1998; 37:3066–3070.
74. Conry RR, Ji GZ, Tipton AA. Inorg Chem. 1999; 38:906–913. [PubMed: 11670862]
75. Reger DL, Collins JE. Organometallics. 1996; 15:2029–2032.
76. Unpublished work.
77. Himes RA, Park GY, Barry AN, Blackburn NJ, Karlin KD. J Am Chem Soc. 2007; 129:5352–5353. [PubMed: 17411054]
78. Pasquali, M.; Floriani, C. Copper(I)-Carbon Monoxide Chemistry: Recent Advances and Perspectives. In: Karlin, KD.; Zubieta, J., editors. Copper Coordination Chemistry: Biochemical & Inorganic Perspectives. Adenine Press; New York: 1983. p. 311-330.
79. Rondelez Y, Seneque O, Rager MN, Duprat AF, Reinaud O. Chem Eur J. 2000; 6:4218–4226.
80. Jonas RT, Stack TDP. Inorg Chem. 1998; 37:6615–6629. [PubMed: 11670793]
81. Fujisawa K, Ono T, Ishikawa Y, Amir N, Miyashita Y, Okamoto K, Lehnert N. Inorg Chem. 2006; 45:1698–1713. [PubMed: 16471983]
82. Dias HVR, Lu HL. Inorg Chem. 1995; 34:5380–&.
83. Carrier SM, Ruggiero CE, Houser RP, Tolman WB. Inorg Chem. 1993; 32:4889–4899.
84. Hu ZB, Williams RD, Tran D, Spiro TG, Gorun SM. J Am Chem Soc. 2000; 122:3556–3557.

85. Zhang CX, Liang HC, Kim EI, Shearer J, Helton ME, Kim E, Kaderli S, Incarvito CD, Zuberbuhler AD, Rheingold AL, Karlin KD. J Am Chem Soc. 2003; 125:634–635. [PubMed: 12526654]

86. τ values (α-β/60°) calculated based on the X-ray crystallographic data reported in cited references.

87. Addison AW, Rao TN, Reedijk J, Vanrijn J, Verschoor GC. J Chem Soc, Dalton Trans. 1984:1349–1356.

88. Karlin KD, Hayes JC, Juen S, Hutchinson JP, Zubieta J. Inorg Chem. 1982; 21:4106–4108.

89. Shearer J, Zhang CX, Zakharov LN, Rheingold AL, Karlin KD. J Am Chem Soc. 2005; 127:5469–5483. [PubMed: 15826184]

90. Smirnov VV, Roth JP. J Am Chem Soc. 2006; 128:3683–3695. [PubMed: 16536541]

91. At much higher O_2 concentrations, the formation of a new Cu-O_2 adduct was observed and will be discussed in a different publication.

92. Metz M, Solomon EI. J Am Chem Soc. 2001; 123:4938–4950. [PubMed: 11457321]

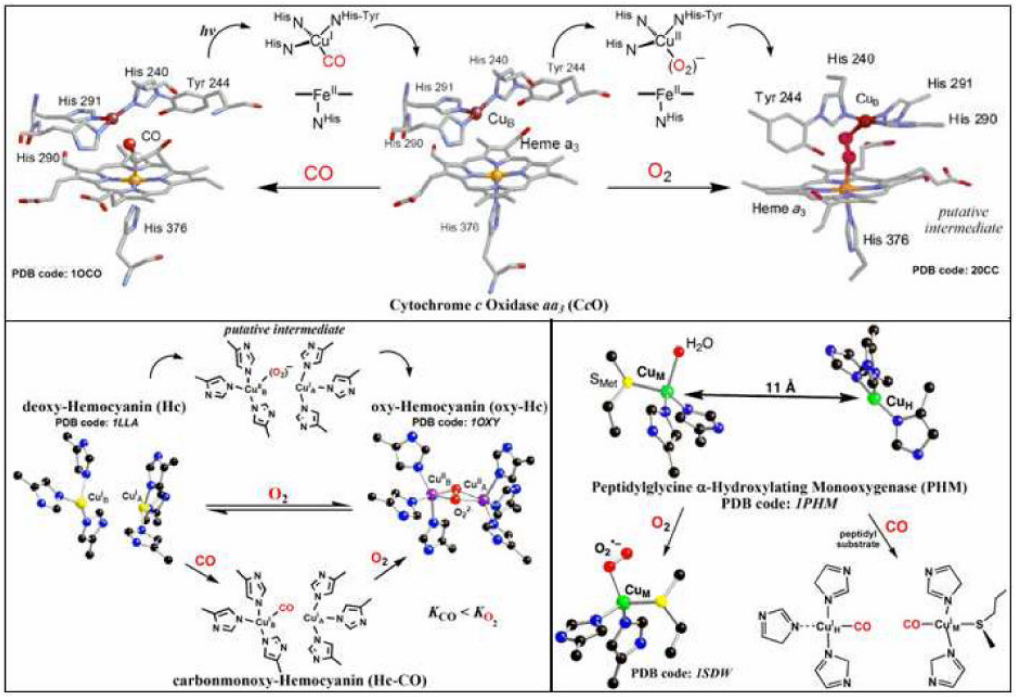

Figure 1.

Overview of reduced copper containing protein active-site O_2 and CO interactions, highlighting the heme$_{a3}$-Cu$_B$ active-site for O_2 binding/reduction of mitochondrial cytochrome *c* oxidase (C*c*O), the arthropodal and molluscan hemolymph O_2-carrier Hc, and the mammalian neuropeptide hormone producing monooxygenase PHM.

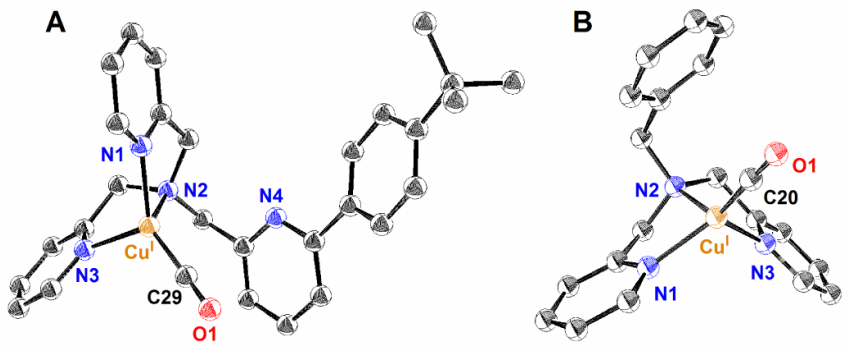

Figure 2.

ORTEP diagrams of **A.** ^{TBP}**LCu^{I}-CO** and **B.** ^{Bz}**LCu^{I}-CO**; hydrogen atoms and the $B(C_6F_5)_4$ counteranion have been omitted for clarity. Selected bond lengths are: **A.** Cu–C 1.801(6) Å, C–O 1.124(6) Å, Cu–$N_{alkylamine}$ 2.147(4) Å, Cu–$N_{pyridine(avg)}$ 2.051(5) Å; and **B.** Cu–C 1.815(1) Å, C–O 1.123(2) Å, Cu–$N_{alkylamine}$ 2.158(6) Å, and Cu–$N_{pyridine(avg)}$ 2.048(3) Å. Selected bond angles are: **A.** C–Cu–$N_{pyridine(avg)}$ 121.4(2)°, C–Cu–$N_{alkylamine}$ 131.0(0)°, $N_{pyridine(avg)}$–Cu–$N_{alkylamine}$ 81.0(9)°, $N_{pyridyl}$–Cu–$N_{pyridyl}$ 109.6(0)°; and **B.** C–Cu–$N_{pyridine(avg)}$ 121.95(7)°, C–Cu–$N_{alkylamine}$ 129.94(7)°, $N_{pyridine(avg)}$–Cu–$N_{alkylamine}$ 80.80(6)°, and $N_{pyridyl}$–Cu–$N_{pyridyl}$ 108.94(6)°.[68]

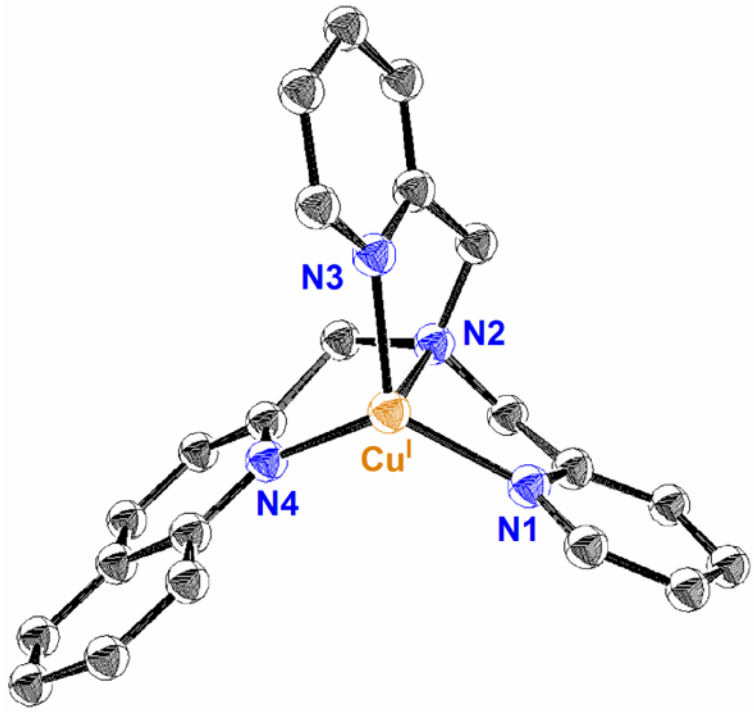

Figure 3.

ORTEP diagram of ^{Q}**LCu**^{I} with hydrogen atoms and the $B(C_6F_5)_4$ counteranion omitted for clarity. Selected bond lengths are: Cu–$N_{pyridine(1)}$ 1.988(2) Å, Cu–$N_{pyridine(3)}$ 2.006(2) Å, Cu–$N_{alkylamine(2)}$ 2.185(2) Å, and Cu–$N_{quinoline(4)}$ 2.012(2) Å. Selected bond angles are: $N_{pyridyl(avg)}$–Cu–$N_{alkylamine(2)}$ 82.84(8)°, $N_{pyridyl(1)}$–Cu–$N_{pyridyl(3)}$ 123.63(8)°, $N_{pyridyl(1)}$–Cu–$N_{quinolyl(4)}$ 119.95(8)°, $N_{amine(2)}$–Cu–$N_{quinolyl(4)}$ 82.58(7)°, and $N_{pyridyl(3)}$–Cu–$N_{quinolyl(4)}$ 111.70(8)°.[68]

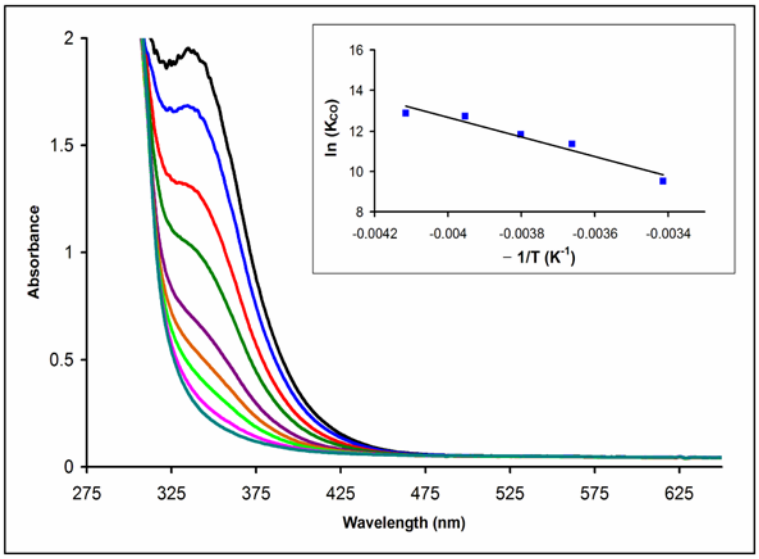

Figure 4.

Spectrophotometric titration of CO to ^{TBP}**LCu**^{I} in THF at room temperature. The inset is a Van't Hoff plot of the variable temperature K_{CO} data collected from −30 °C to +20 °C.

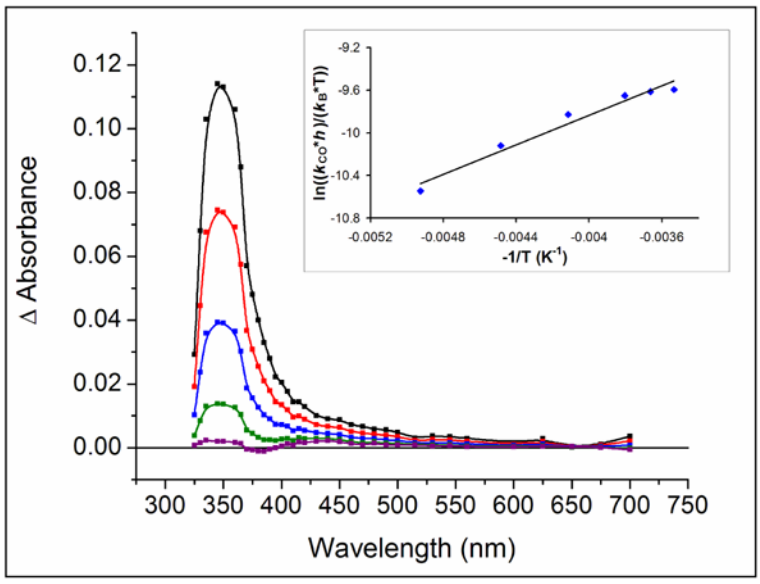

Figure 5.

Transient absorption difference spectra observed after pulsed 355 nm excitation of ^{TBP}**LCu^{I}-CO** in THF at room-temperature under 1 atm of CO. CO photodissociation and the formation of ^{TBP}**LCu^{I}** followed by subsequent CO recombination is measured and shown at various delay times: 0 ns (black); 100 ns (red); 250 ns (blue); 500 ns (green); 1000 ns (purple). The inset is an Eyring analysis plot of the k_{CO} data collected at variable temperature (−70 °C to 10 °C).

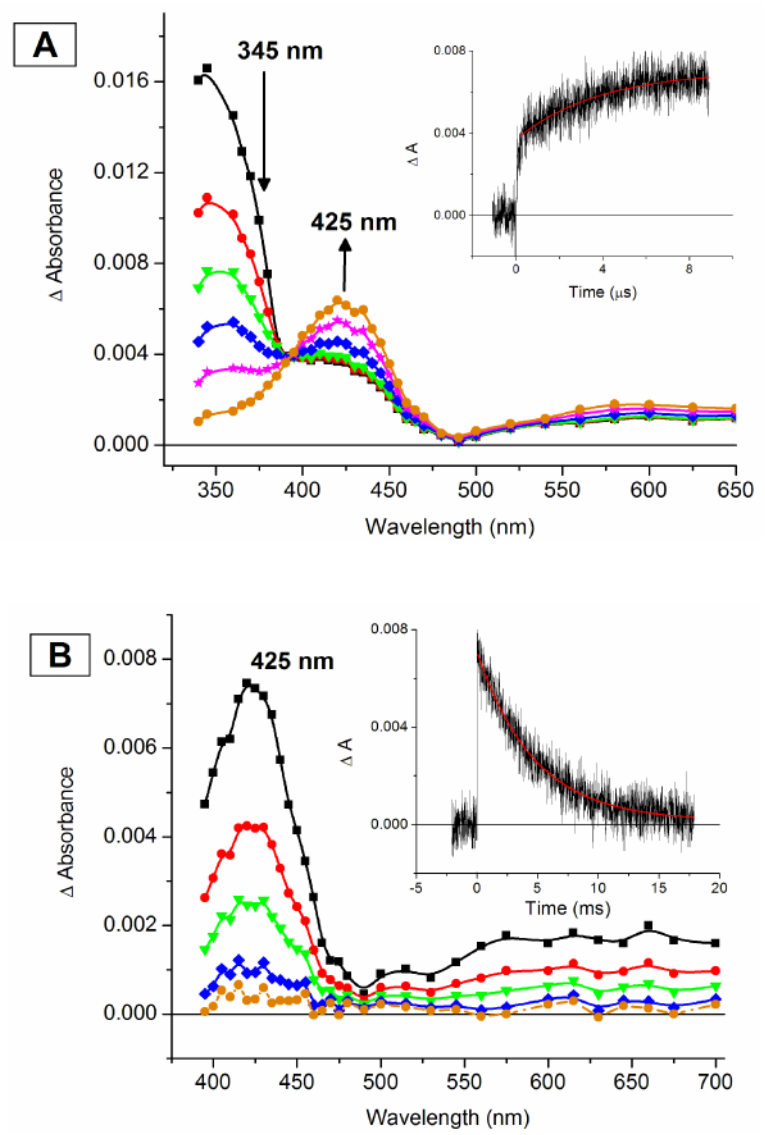

Figure 6.

Absorption difference spectra [^{NMe2}**LCu**$^{I/II}$-**X** – ^{NMe2}**LCu**^{I}-**CO**] recorded after pulsed λ_{ex} =355 nm excitation of ^{NMe2}**LCu**^{I}-**CO** in THF at 193 K under 1 atm O_2:CO (1:1) mixture. The spectra were recorded at various delay times: (**A**) 0 to 5 μs representing the conversion of ^{NMe2}**LCu**^{I} to a mixture of ^{NMe2}**LCu**^{I}-**CO** and ^{NMe2}**LCu**^{II}-**O**$_2^-$: black squares, 0 μs; red circles, 0.1 μs; green triangles, 0.25 μs; blue diamonds, 1 μs; magenta stars, 2.5 μs; orange circles, 5.0 μs. The inset is an absorption transient monitored at 425 nm with a superimposed first-order fit (in red), k_{obs} = 2.92 × 10^5 s^{-1} and (**B**) 0 ms to 20 ms representing the conversion from ^{NMe2}**LCu**^{II}-**O**$_2^-$ to ^{NMe2}**LCu**^{I}-**CO**: black squares, 0 ms; red circles, 2.5 ms; green triangles, 5.0 ms; blue diamonds, 10 ms; orange circles, 20 ms. The inset is an absorption transient monitored at 425 nm with a superimposed first-order fit (in red), k_{obs} = 236 s^{-1}.

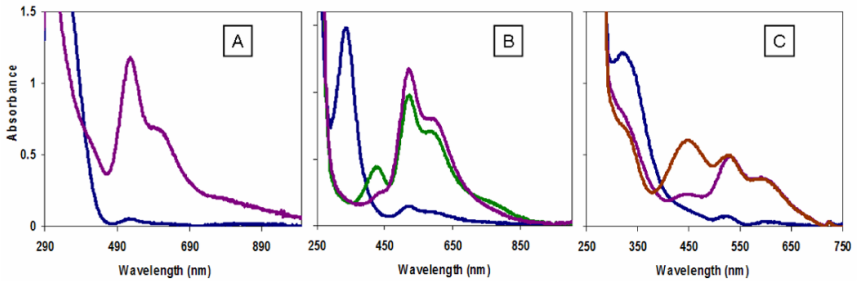

Figure 7.

UV-visible spectra in MeTHF at −128 °C representing O_2 + ^{D}**LCu^{I}** (dark blue) to yield: A, [{(^{Im}L)Cu^{II}}$_2$(O_2^{2-})]$^{2+}$ (purple); B, ^{Py}**LCu^{II}-O$_2^-$** (green) and [{(^{Py}L)Cu^{II}}$_2$(O_2^{2-})]$^{2+}$ (purple); C, [{(^{NMe2}L)Cu^{II}}$_2$(O_2^{2-})]$^{2+}$ (purple) and a new copper-dioxygen adduct of ^{NMe2}**L** (brown).

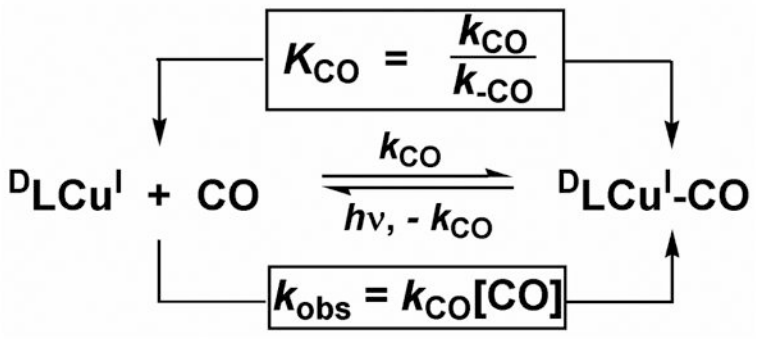

Scheme 1.

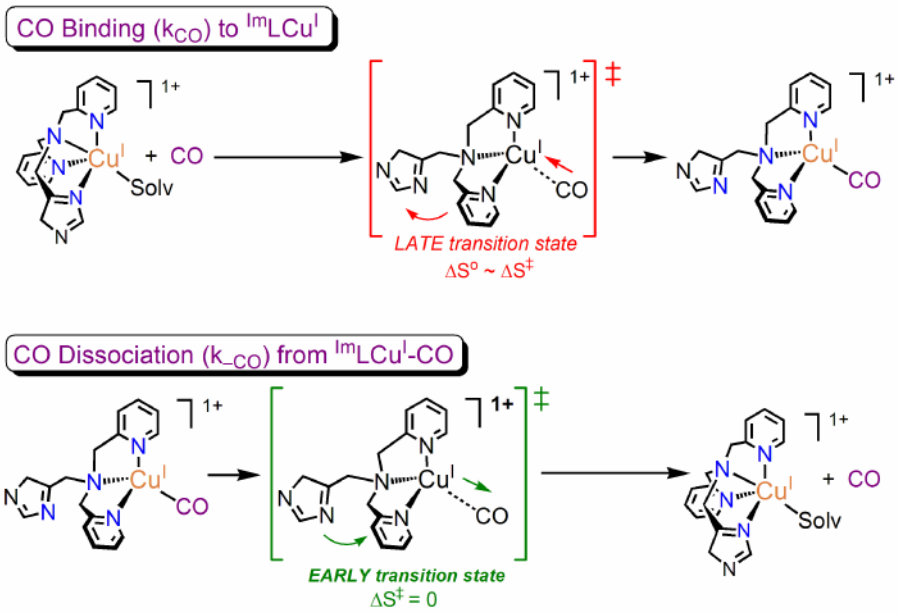

Scheme 2.

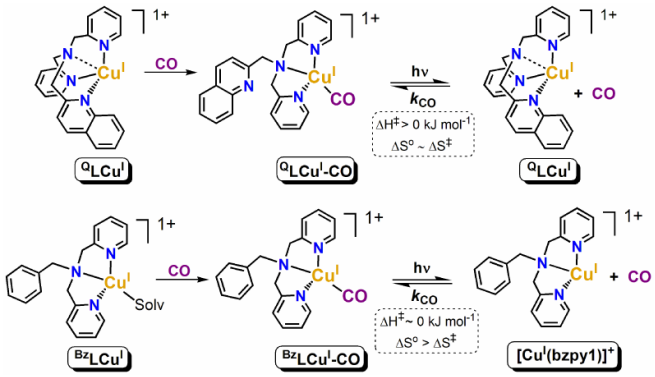

Scheme 3.

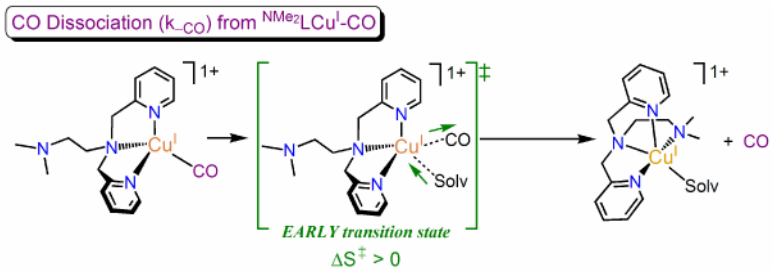

Scheme 4.

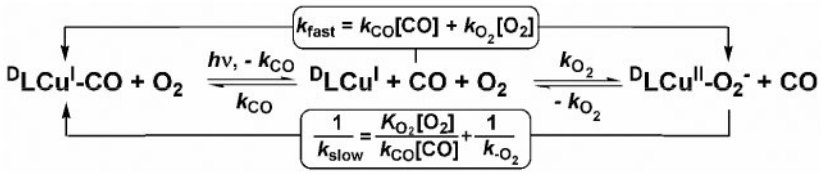

Scheme 6.

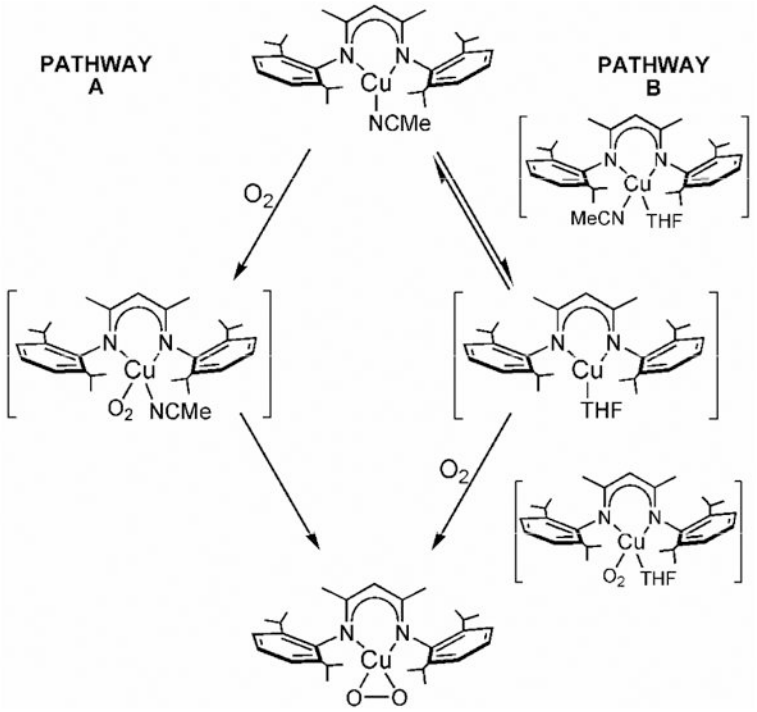

Scheme 7.

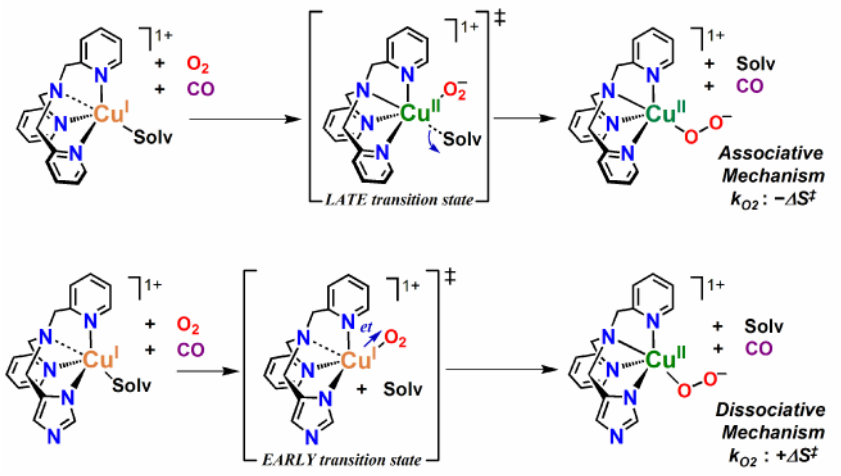

Scheme 8.

Smirnov and Roth:

Suggested Here:

Scheme 9.

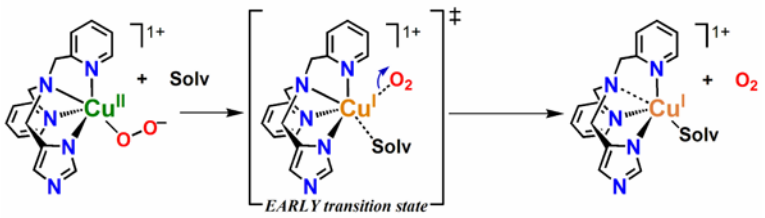

Scheme 10.

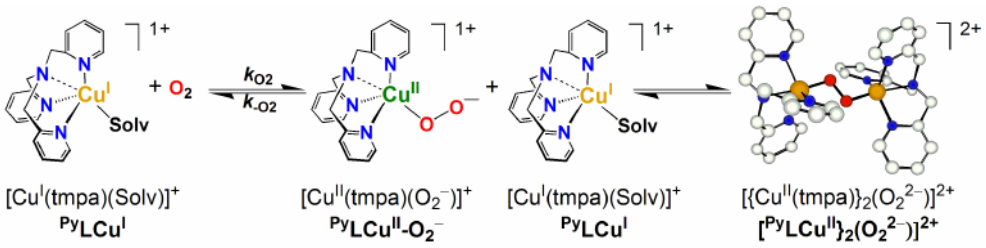

Scheme 11.

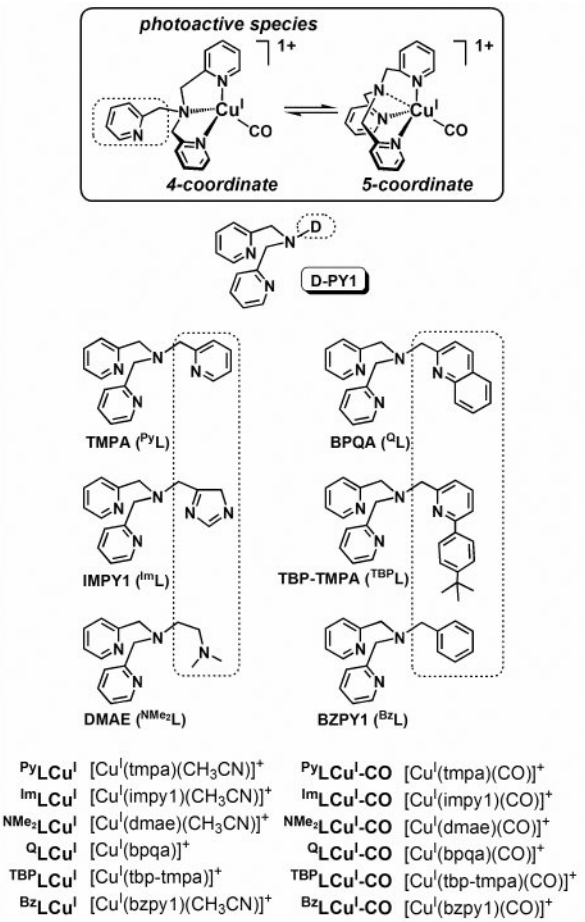

Chart 1.

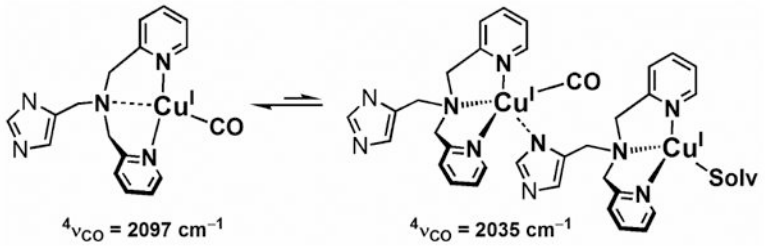

Chart 2.

Table 1

Carbonyl Stretching Frequencies for ^{D}**LCu^{I}-CO** Complexes and Cyclic Voltammetry Data for ^{D}**LCu^{I}** Complexes.

Compound	Neat solid	THF solution	$E_{1/2}$ *b*	ΔE *b*
^{Im}LCu^{I}-CO	2097, 2035$_{(sm)}$	2087, 2063	−445	110
^{NMe2}LCu^{I}-CO	2097	2090	−445	85
^{Py}LCu^{I}-CO	2077	2091, 2074$_{(sh)}$	−410	75
^{Q}LCu^{I}-CO	2090	2091	−325	110
^{TBP}LCu^{I}-CO	2091	2092	−325	115
^{Bz}LCu^{I}-CO	2093	2093	−225	155

a Abbreviations are as follows: sm = small, sh = shoulder.

b Electrochemical measurements are of copper(I) complexes (not carbonyl) in deoxygenated CH_3CN. Potentials are reported versus the Fc^{+}/Fc redox couple and are rounded to the nearest 5 mV.

Table 2

Kinetic and Thermodynamic Parameters for CO binding to ^{D}**LCu**^{I} in THF; Constants Reported at 298 K.[a]

Compound	K_{CO} (M^{-1})	ΔH°	ΔS°	k_{CO} (M^{-1} s^{-1})	ΔH‡	ΔS‡	k_{-CO} (s^{-1})	ΔH‡	ΔS‡
^{Im}**LCu**^{I}**-CO**	(2.4 ± 0.04) × 10^3	−31.4	−40.6	(2.8 ± 0.07) × 10^9	7.03	−40.5	(1.1 ± 0.04) × 10^6	38.5	0.1
^{NMe2}**LCu**^{I}**-CO**	(5.0 ± 0.05) × 10^3	−39.7	−62.5	(2.5 ± 0.05) × 10^9	9.07	−34.7	(5.0 ± 0.09) × 10^5	48.8	28
^{Py}**LCu**^{I}**-CO**	(1.2 ± 0.05) × 10^4	−35.9	−42.6	(1.9 ± 0.02) × 10^9	7.13	−43.3	(1.5 ± 0.04) × 10^5	43.0	−0.7
^{Q}**LCu**^{I}**-CO**	(2.2 ± 0.2) × 10^4	−39.2	−48.5	(9.7 ± 0.1) × 10^8	5.66	−53.9	(4.4 ± 0.01) × 10^4	44.9	−5.3
^{TBP}**LCu**^{I}**-CO**	(1.4 ± 0.03) × 10^4	−40.4	−56.2	(5.2 ± 0.01) × 10^8	5.76	−58.7	(3.7 ± 0.01) × 10^4	46.2	−2.5
^{Bz}**LCu**^{I}**-CO**	(5.6 ± 0.1) × 10^4	−46.0	−63.6	(5.0 ± 0.01) × 10^8	0.74	−75.9	(9.0 ± 0.03) × 10^3	46.8	−76

[a] Units of kinetic and thermodynamic values are as follows: K_{CO}, M^{-1}; k_{CO}, M^{-1} s^{-1}; k_{-CO}, s^{-1}; **ΔH**, kJ mol^{-1}; **ΔS**, J mol^{-1} K^{-1}. See Supporting Information for Van't Hoff and Eyring plots.

Table 3

Comparison of the kinetics and thermodynamics for formation of $^{D}LCu^{II}\text{-}O_2^{-}$ (**D = Py, Im, NMe_2**) in THF and other ligand-copper(II)-η^1-superoxo species.

Parameter	$^{Py}LCu^{I}$ THF[(a)]	$^{Py}LCu^{I}$ EtCN[(b)]	$[Cu^{I}(Me_6tren)]^{+}$ EtCN[(b)]	$^{Im}LCu^{I}$ THF[(c)]	$^{NMe2}LCu^{I}$ THF[(c)]
k_{O2}, 193 K (M^{-1} s^{-1})	$(1.5 \pm 0.02) \times 10^{8}$	$(3.8 \pm 0.01) \times 10^{4}$	$(1.8 \pm 0.04) \times 10^{5}$	$(1.8 \pm 0.03) \times 10^{8}$	$(6.9 \pm 0.02) \times 10^{7}$
k_{O2}, 298 K (M^{-1} s^{-1})	$(1.3 \pm 0.02) \times 10^{9}$	$(5.8 \pm 0.8) \times 10^{7}$	$(1.2 \pm 0.1) \times 10^{7}$	$(3.4 \pm 0.6) \times 10^{10}$	$(2.3 \pm 0.4) \times 10^{11}$
$\Delta H^{\ddagger}$ (kJ mol^{-1})	7.62	31.6	17.1	23.4	32.1
$\Delta S^{\ddagger}$ (J mol^{-1} K^{-1})	− 45.1	10	− 52	35.1	80.1
k_{-O2}, 193 K (s^{-1})	240 ± 6	130 ± 1	0.62 ± 0.01	1600 ± 0.05	470 ± 0.02
k_{-O2}, 298 K (s^{-1})	$(1.3 \pm 0.03) \times 10^{8}$	$(1.5 \pm 0.2) \times 10^{8}$	$(7.7 \pm 0.9) \times 10^{5}$	$(1.9 \pm 0.2) \times 10^{9}$	$(2.3 \pm 0.3) \times 10^{9}$
$\Delta H^{\ddagger}$ (kJ mol^{-1})	58.0	61.5	62.0	64.5	66.5
$\Delta S^{\ddagger}$ (J mol^{-1} K^{-1})	105	118	76	150	157
K_{O2}, 193 K (M^{-1})	$(6.5 \pm 0.02) \times 10^{5}$	260 ± 4	$(2.9 \pm 0.04) \times 10^{5}$	$(1.1 \pm 0.03) \times 10^{5}$	$(1.5 \pm 0.06) \times 10^{5}$
K_{O2}, 298 K (M^{-1})	15.4 ± 0.3	0.38 ± 0.02	15.5 ± 0.5	17.4 ± 0.8	100 ± 0.7
$\Delta H°$ (kJ mol^{-1})	− 48.5	− 29.8	− 44.9	− 41.1	− 34.4
$\Delta S°$ (J mol^{-1} K^{-1})	− 140	− 108	− 128	− 114	− 77.3

O_2 binding data was previously published and collected through

[(a)] flash-and-trap techniques in THF,[15]

[(b)] stopped-flow spectroscopy in EtCN.[14,85]

[(c)] Averaged values were determined from analysis of k_{slow} using the flash-and-trap methods discussed herein, see text for more details. Bimolecular k_{O2} values calculated at additional temperatures are given in the Supporting Information, Table S2.

Table 4

Comparison of CO and O_2 Bimolecular Rates and Binding Constants at 298 K for Select Ligand-Copper(I)-Complexes, Hemocyanins (Hc), and Selected Hemes.

Compound or Protein	K_{CO} (M^{-1})	K_{O2} (M^{-1})	k_{CO} (M^{-1} s^{-1})	k_{O2} (M^{-1} s^{-1})	k_{-CO} (s^{-1})	k_{-O2} (s^{-1})
$^{NMe2}LCu^{I}$ (THF)	4.9×10^3	100	2.5×10^9	2.3×10^{11}	5.0×10^5	2.3×10^9
$^{Im}LCu^{I}$ (THF)	2.4×10^3	17.4	2.8×10^9	3.4×10^{10}	1.1×10^6	1.9×10^9
$^{Py}LCu^{I}$ (THF)	1.2×10^4	15.4	1.9×10^9	1.3×10^9	1.6×10^5	1.3×10^8
$^{Py}LCu^{I}$ (CH_3CN)	220	0.38	5.9×10^7	5.8×10^7	2.7×10^5	1.5×10^8
Myoglobin (human)	2.6×10^7	$(0.74–117) \times 10^4$	7.6×10^5	$(1.4–25) \times 10^7$	0.022	22
Hemoglobin (human)	4.6×10^8	$(2.9–48) \times 10^5$	4.6×10^6	$(2.9 –22) \times 10^7$	0.009	13.1
Limulus Hc (arthropod)	$(2.7 – 11.2) \times 10^3$	$(2.6 – 5.4) \times 10^5$	$(2 – 4.3) \times 10^5$	$(1.3 – 1.9) \times 10^6$	38 – 75	2.4 – 7.5
Busycon Hc (mollusk)	220×10^3	1.8×10^5	7.7×10^5	$(1.1 – 2.2) \times 10^6$	3 – 4	6.5 – 11.5

J Am Chem Soc. Author manuscript; available in PMC 2011 September 22.